ecologies

MDPI

Article

Formation and Ecological Dynamics of Synthetic Biofilms Derived from Microbial Components of the *Cladonia arbuscula* Thallus

Timofey A. Pankratov * and Armen V. Hakobjanyan

S.N. Winogradsky Institute of Microbiology, Research Centre of Biotechnology of RAS, 119071 Moscow, Russia; hakobjanyanarmen0@gmail.com

* Correspondence: tpankratov@gmail.com or t.pankratov@inmi.ru

Abstract

Synthetic multi-species consortia provide valuable insights into the ecological and structural dynamics of complex microbial biofilms. However, the specialized functional contributions of individual components under severe nutrient limitations remain poorly understood. This study investigated the population dynamics, matrix biogenesis and metabolic potential of a synthetic 'protolichen biofilm' model comprising *Asterochloris* microalgae, *Gordonia* bacteria, *Thelebolus* filamentous fungi and *Occultifur* yeast. The biofilms were cultivated under strict carbohydrate-deficient conditions for 30 days. Population changes, extracellular polymeric substance (EPS) matrix formation, and the concentrations of extracellular DNA (exDNA) and proteins (exProt), as well as potential dehydrogenase activity (via iodonitrotetrazolium reduction), were evaluated across monocultures, binary, ternary and quaternary consortia. Under carbon starvation, the photoautotrophic microalgae dominated the consortium, driving an 11-fold increase in population size in the four-component system and serving as the primary source of exDNA, which increased by up to three orders of magnitude by day 30. The *Gordonia* sp. exhibited a tenfold expansion by actively localizing to fungal hyphae and microalgal cell walls. This was directly correlated with a sharp increase in metabolic activity. By contrast, *Thelebolus* sp. initially provided the structural framework via EPS production, but exhibited limited metabolic activity over time. Meanwhile, the *Occultifur* sp. yeast population was severely suppressed, adopting a sit-and-wait ecological strategy. Spearman correlation analysis revealed that multi-species integration stabilized the community and triggered significant emergent effects in exDNA accumulation and metabolic potential, but only when microalgae were present. These findings demonstrate that microalgae and bacteria primarily drive metabolism and regulation within the protolichen consortia investigated, while fungi and yeast play structural or opportunistic roles. This provides a robust framework for understanding complex symbiotic interactions.

Keywords: multi-species biofilms; synthetic consortia; protolichen model; extracellular DNA; metabolic potential; interspecific competition; *Cladonia arbuscula*

Check for updates

Academic Editor: José Ramón Arévalo Sierra

Received: 28 July 2026
Revised: 28 August 2026
Accepted: 28 August 2026
Published: 2 September 2026

Copyright: © 2026 by the authors. Licensee MDPI, Basel, Switzerland. This article is an open access article distributed under the terms and conditions of the Creative Commons Attribution (CC BY) license.

1. Introduction

Lichens are complex multiorganism entities. When thalli form from spores rather than soredia or isidia, the initial stages of self-organization occur at the level of biofilms consisting of fungal mycelium (mycobionts), algae and associated microorganisms such as bacteria, yeasts and free-living fungi. These microbial biofilms play a key role in ecosystem function and the stabilization of complex microbial community functions [1–3].

Molecular exchange processes in biofilm structures differ from those in planktonic cultures [4]. This is a consequence of the formation of a matrix, the role of which in the functioning of biofilms is the subject of ongoing research [5], as is the spatial stabilization of cells [6,7]. Lichens are well-structured 3D biofilms [8,9], combining features of a superorganism (holobiont) and an ecosystem [10,11]. In their mature state, the secondary thalli (podetia) of lichens form clearly distinguishable morphotypes, the formation mechanism of which remains poorly understood in the study of lichen physiology and ecology. In the early stages of development, prior to the formation of mature podetia, the binary biofilm forms a scaly primary thallus that resembles a mature binary biofilm more closely. The formation of the secondary thallus is triggered by environmental factors such as drying and wetting, and by secondary metabolites produced by the fungus and alga. These metabolites likely play a decisive role [12].

Reconstructing lichen symbioses is a complex task that has been the subject of research for many years. The field was pioneered by Ahmadjian's group [12–15]. Today, as in the past, attempts to artificially recreate the lichen thallus persist [16,17]. The as-yet-unknown mechanisms of chemical and 'immune' interactions between the mycobiont and photobiont that lead to stable symbiosis stand in the way of solving this problem, as do the difficulties associated with maintaining the mycobiont in an axenic culture. However, data from metagenomic and metatranscriptomic analyses are beginning to emerge which attribute a leading role in forming the symbiotic relationship to enzymes, polysaccharides and secondary metabolites [16,18,19].

Nevertheless, the question of which processes occur during the formation of complex biofilms involving fungi, algae and bacteria remains unanswered.

Microorganisms that are associated with thallus formation and that are almost always present in lichen thalli have been isolated [20–22]. The localization of these associated microorganisms can vary, with them being either epibionts or microorganisms located within the thallus [23–25]. These include Gram-positive and Gram-negative bacteria [26], filamentous fungi [27,28], algae [29] and yeasts [25]. As with any complex system, an increase in the number of components leads to changes in metabolism and an increase in communication channels, primarily chemical, between the various components of the system [30,31]. The increasing complexity of a system comprising a multidomain complex of species can result in an emergent effect, whereby the characteristics of the complex system differ from those of its individual components [32,33].

As culturing the mycobiont of a lichen can be challenging and the reconstruction of the lichen thallus unpredictable, an alternative approach is to co-cultivate the photobiont alongside microorganisms isolated from the thallus's internal structures (e.g., endolichenic fungi, bacteria and yeasts). Such cultures are characterized by stable growth, and the biofilms they form can serve as (albeit imperfect) models of the biofilms formed with the participation of mycobionts [34]. Several conditions are necessary to simulate those under which the biofilms that form primary thalli develop. Firstly, the mycobiont and photobiont must work together to form a matrix by synthesizing extracellular polymers. Secondly, the growth rates and temperature conditions of all components must be consistent. Thirdly, the accompanying microorganisms must also meet these conditions, namely a low growth rate and a similar optimal temperature. Finally, the mineral composition of the dense medium or solid surface should replicate natural conditions, with a low concentration of free inorganic ions, an optimal pH and a low concentration of organic compounds. All components of the biofilm must be capable of growing on nutrient-limited media.

Traditional methods of assessing biofilm development include measuring biofilm density, structure, degree of microbial cell aggregation and matrix composition and density [35,36]. Key characteristics for assessing biofilm development include the concentration

of extracellular nucleic acids and proteins, as well as dehydrogenase (respiration) activity. Comprehensive assessments of biofilm morphology are performed using scanning electron microscopy and fluorescence (confocal) microscopy [37–39].

During the preliminary stages of our research [25,40], we isolated cultures of fungi, algae, bacteria and yeast from the lichen species *Cladonia arbuscula*. We selected the filamentous fungus *Thelebolus* sp., the microalga *Asterochloris* sp., the bacterium *Gordonia* sp. and the yeast *Occultifur* sp. from the cultures that met the aforementioned conditions for biofilm formation. These species were further characterized by sequencing specific genes (ITS, 18S rRNA and 28S rRNA for fungi; 23S mitochondrial rRNA for algae; and 16S rRNA for bacteria) to support their taxonomic assignments. Additional selection criteria included *Thelebolus* sp.'s ability to form a dense extracellular polymeric matrix with a gel-like consistency, the hydrophobicity of *Gordonia* sp. cells and reports that *Occultifur* yeasts are frequently associated with lichens due to their mycophily and mycoparasitism [41].

This study aimed to reconstruct and investigate the growth rate and metabolic activity of monospecific and complex biofilms, and to examine their morphology and structure over time, transitioning from early (5-day) to mature (30-day) stages. The main objective was to elucidate the role of individual components in biofilm development and function, as well as to identify emergent properties within complex, multidomain systems.

2. Materials and Methods

2.1. Culture Isolation and Maintenance

The formation of biofilms was achieved through the use of bacterial, yeast, fungal and algal cultures that had been isolated from the lichen *Cladonia arbuscula* (Wallr.) Flot. collected in Naryan-Mar, Russia [40]. These included the bacterium *Gordonia* sp. strain NM9-41, the yeast *Occultifur* sp. strain 7.1.2.11, the filamentous fungus *Thelebolus* sp. strain 7.1.2.4, and the microalga *Asterochloris* sp. strain 11A1 (Figures 1 and S1–S4). Axenic cultures of the bacteria, yeast, and fungi were grown on FA+ medium [40] at 20 °C. The algae were maintained on Bold's Basal Medium [42] at 20 °C under a 12:12 h light/dark cycle.

2.2. Culture Identification

The cultures were identified using standard molecular methods with primers previously described for fungi [43–45], bacteria [46], and algae [47]. Sanger sequencing was performed on a 3730 DNA Analyzer (Applied Biosystems, Waltham, MA, USA). We assembled the sequence data into contigs using UGENE (version 52.0). Subsequent sequence alignment, trimming, marker gene analysis, and phylogenetic tree construction were carried out in MEGA X [48]. Phylogenetic trees were inferred using the Maximum Likelihood method based on the Jukes–Cantor model, with topological support evaluated via bootstrap analysis (1000 replications). The GenBank accession numbers were PZ807577, PZ834537, PZ807174 and PZ838513 for the bacterium *Gordonia*, the yeast *Occultifur*, the filamentous fungus *Thelebolus*, and the microalga *Asterochloris*, respectively.

2.3. Preparation of Microbial Suspensions

The key steps of the sample preparation workflow are illustrated in Figure 2. Suspensions were prepared using cultures of specific ages: 5 days for bacteria and yeast, 10 days for fungi, and 20 days for algae. For biomass collection, either two bacteriological loops (V = 2 μL) of material (for bacteria, yeast, and algae) or half of a fungal mycelial colony (1 cm in diameter) were transferred into 1 mL of sterile deionized water (dH_2O). The mixture was homogenized using a Bioprep-6 homogenizer (Allsheng, Hangzhou, China) at 6 m/s for 30 s (two cycles with a 30-s interval). The resulting homogeneous mixtures were transferred to 15 mL Falcon tubes, and the total volume was adjusted to 4 mL with dH_2O.

These stock suspensions were used to prepare specific dilutions for biofilm inoculation. For monocultures, the dH_2O-to-suspension ratio was 1:3 (v/v); for binary and ternary biofilms, the ratios were 1:1 and 3:1 (v/v), respectively. For quaternary biofilms, undiluted stock suspensions were deployed. Finally, the mixtures were vortexed using a Vortex V-3 (20 s, 3000 rpm) and applied onto hydrophilic nylon filters (25 mm diameter, 0.45 µm pore size; Merck Millipore, Darmstadt, Germany, HNWP02500).

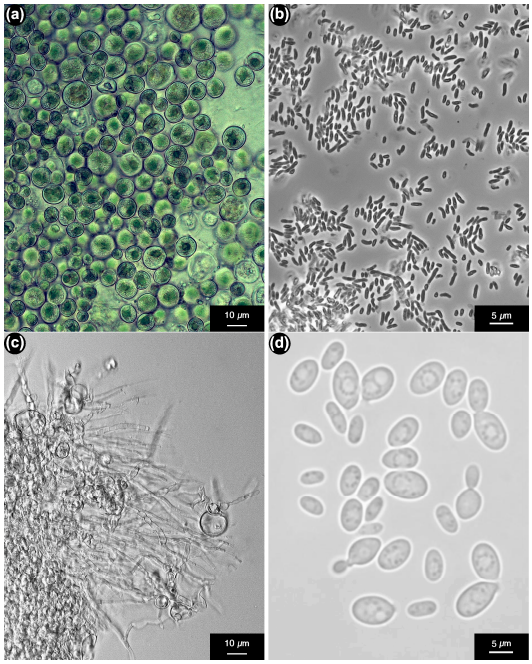


Figure 1. Light microscopy morphology of microbial cultures used for biofilm formation. Images captured using distinct illumination techniques: (**a**) *Asterochloris* sp. strain 11A1 and (**c**) *Thelebolus* sp. strain 7.1.2.4 visualized under bright-field microscopy with oblique (off-axis) illumination; (**b**) *Gordonia* sp. strain NM9-41 and (**d**) *Occultifur* sp. strain 7.1.2.11 visualized under phase-contrast microscopy. Samples were prepared as native wet mounts. Scale bars: (**a**,**c**) =10 µm; (**b**,**d**) =5 µm.

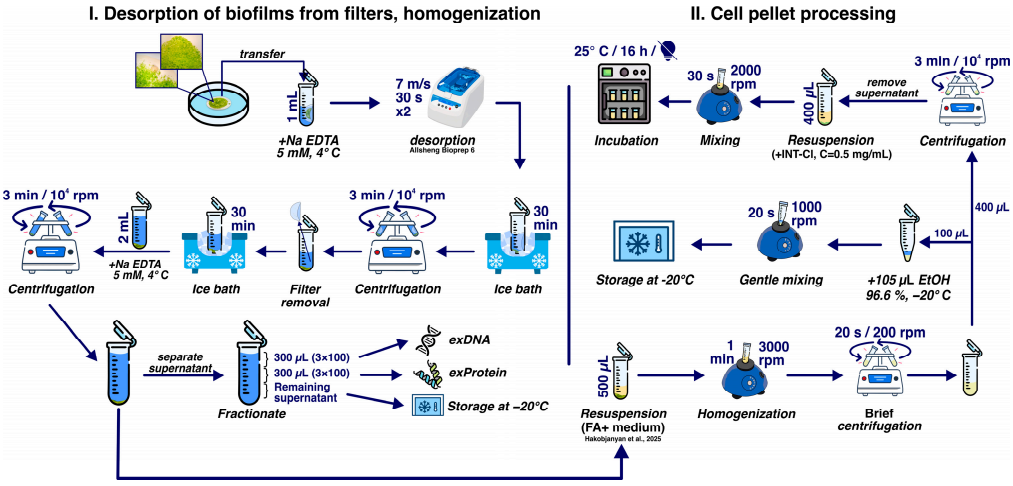


Figure 2. Schematic workflow of sample preparation for biofilm analysis. The procedure is divided into two main stages: (**I**) desorption of biofilms from filters and homogenization, leading to supernatant fractionation for extracellular polymeric substances (EPS) analysis (exDNA and exProtein isolation); and (**II**) processing of the remaining cell pellet, including incubation with iodonitrotetrazolium chloride (INT-Cl) for metabolic activity assessment. The resuspension step in stage II is performed using liquid FA+ medium according to [40].

2.4. Biofilm Inoculation and Cultivation

For all experimental variants, a fixed total volume of 120 µL of microbial suspension was inoculated onto each nylon filter. This total volume was divided equally among the respective constituents: 120 µL for monospecific biofilms, 60 µL per constituent for binary biofilms, 40 µL for ternary biofilms, and 30 µL for quaternary biofilms. The multi-component mixtures were pre-assembled in 1.5 mL tubes before being pipetted onto the filters. The filters were placed in Petri dishes containing agar-solidified media. All biofilm variants were prepared in triplicate. The composition of the culture medium was as follows (g/L): $(NH_4)_2SO_4$, 0.05; KH_2PO_4, 0.05; $MgSO_4 \times 5H_2O$, 0.025; NaCl, 0.015; glucose, 0.05; microelements (mg/L: $MnSO_4 \times H_2O$, 5; $FeSO_4 \times 7H_2O$, 5; $CoCl_2 \times H_2O$, 2; $ZnSO_4 \times 7H_2O$, 2; $CuSO_4 \times 5H_2O$, 1; $Na_2MoO_4 \times 2H_2O$, 1; $NiCl_2 \times 6H_2O$, 0.1); vitamins (µg/L: p-aminobenzoate, 40; biotin, 5; nicotinic acid, 50; thiamine-HCl $\times 2H_2O$, 40; pyridoxamine, 125; cyanocobalamin, 50; pantothenic acid, 12); and agar-agar for microclonal plant propagation and microbiology, 1000 g/cm^2 (Angel Yeast Co., Yichang, China), 10 g/L.

2.5. Incubation and Sampling

The biofilms were incubated at 20 ± 2 °C under a 12:12 h light/dark cycle for 30 days. Illumination was provided by a FITO-18W-PL LED lamp (ERA, St. Petersburg, Russia; wavelengths: 445–450 nm and 660 nm; photon flux: 36 µmol/s). To minimize moisture loss from the agar medium, the Petri dishes were enclosed in ventilated plastic bags; the total weight loss of the dishes due to evaporation did not exceed 8% over the entire incubation period. Biofilm samples were harvested for analysis on days 5, 10, 20, and 30 of the experiment.

2.6. Biofilm Desorption and Homogenization

Each filter was removed from the agar plate using sterile forceps and transferred to a 2 mL microcentrifuge tube, ensuring the biomass-free side faced the tube wall. Next, 1 mL of ice-cold (4 °C) 5 mM $Na_4EDTA \times 4H_2O$ solution (pH 8.0) was added. Biomass desorption was performed using a Bioprep-6 homogenizer (Allsheng, Hangzhou, China) at 6 m/s for two 30-s cycles. Complete cell removal was verified visually; when necessary, the homogenization cycle was repeated.

The tubes were placed in an ice bath and incubated for 30 min. The filters were then carefully removed, and the remaining suspensions were centrifuged (3 min, 6700× *g*, 4 °C) to pellet the cells and fungal mycelium. The pellet was resuspended, and the total volume was adjusted to 2 mL with ice-cold 5 mM $Na_4EDTA \times 4H_2O$. Following a second round of centrifugation under the same conditions, the sample was split into aliquots: 300 µL was collected for nucleic acid analysis, and the same volume was allocated for protein assay (further subdivided into three 100 µL technical replicates). The remaining volume was stored at −20 °C.

2.7. Processing of the Cell Pellet and Metabolic Activity Assay

The resulting cell pellet was resuspended and homogenized in 500 µL of liquid FA+ medium [40] using a Vortex V-3 mixer (ELMI, Riga, Latvia) (3000 rpm, 1 min). Droplets adhering to the tube walls were collected by brief centrifugation (200 rpm, 10 s). A 100 µL aliquot of this suspension was transferred to a 1.5 mL tube, mixed with 105 µL of chilled −20 °C 96.6% ethanol (1000 rpm, 20 s), and stored at −20 °C until further use.

The remaining 400 µL of the suspension was centrifuged (6700× *g*, 3 min), and the supernatant was discarded. The remaining pellet was resuspended in 400 µL of liquid FA+ medium containing 0.5 mg/mL iodonitrotetrazolium chloride (INT-Cl; Merck) and mixed thoroughly (2000 rpm, 30 s). The samples were then incubated at 25 °C for 16 h in

the dark. After incubation, the samples were prepared for the colorimetric determination of formazan concentration.

2.8. Intracellular Activity Assay via INT-Cl Reduction

Following incubation with INT-Cl, the cell suspensions were centrifuged (3 min, 6700× *g*), and the supernatant was discarded. The resulting pellet was resuspended in 400 µL of 100% DMSO (molecular biology grade; AppliChem, Darmstadt, Germany) by vortexing (30 s, 2000 rpm). Formazan extraction was allowed to proceed for 15 min at room temperature. The suspension was vortexed again and centrifuged under the same conditions to pellet cell debris. The supernatant containing the extracted formazan was transferred to a 96-well plate (200 µL per well). Absorbance was scanned at 440, 458, 666, and 788 nm using a Feyond A300 microplate reader (Allsheng, Hangzhou, China). Since the maximum absorbance peak was detected at 458 nm, this wavelength was selected for all subsequent quantitative analyses.

2.9. Microscopy, Cell Counting, and Mycelium Volume Estimation

Following vigorous homogenization in the Bioprep-6 system, a 1 µL aliquot of the fixed sample was withdrawn from the 200 µL stock and mixed with 9 µL of distilled water pre-dispensed onto the well (6 mm diameter) of a Teflon-coated microscope slide. The mixture was evenly spread across the well area using a titanium loop (1 mm diameter) and air-dried at room temperature. For cell counting, a drop of Vaseline oil was applied to each well, and the slide was enclosed with a coverslip.

Microscopic evaluation was conducted under transmitted light and phase-contrast modes using an Axio Imager D1 microscope (Carl Zeiss, Oberkochen, Germany). Micrographs were captured at a total magnification of 630× using a digital camera operated via the VideoZavr software package (v. 2.4, St. Petersburg, Russia). The field of view was 18,115 µm^2. The number of cells per filter was calculated using the following conversion formula: $((2.83 \times 10^7 \times N)/18{,}115) \times 1000$, where N is the number of cells or the mycelium volume within the field of view. The mycelium volume was calculated using the cylinder volume formula after measuring its average total length and diameter (AxioVision Rel. 4.8). Bacterial and yeast cells were counted in 20 fields of view per replicate. The algal cell count, as well as the mycelium length and volume, was determined in 40 fields of view for each of the three biological replicates. Mycelium volume was converted to biomass using previously described formulas [49]. All culture images were acquired using a fluorescence, bright-field, phase-contrast and oblique (off-axis) illumination-equipped Axio Imager D1 microscope (Carl Zeiss, Oberkochen, Germany).

2.10. Preparation of Filters for Scanning Electron and Fluorescence Microscopy

Biofilms sampled at 5 and 30 days were analyzed. Biofilm fixation was performed according to the method described by Wells et al. [50], with minor modifications. The filter containing the biofilm was immersed in a 2.5% glutaraldehyde solution for four hours. It was then carefully rinsed with distilled water via pipetting to prevent cells from being dislodged from the filter surface. Any excess moisture was then removed using filter paper and the filter was dehydrated through a graded ethanol series (50%, 70% and 100%). The resulting specimens were then allowed to air-dry completely.

2.10.1. Scanning Electron Microscopy (SEM)

For SEM analysis, a fragment of the biofilm was gold-sputtered using a JEOL Fine Coat Ion Sputter JFC-1100 (JEOL, Tokyo, Japan). The sample stubs were then loaded into the chamber of a JEOL JSM-IT200 scanning electron microscope (JEOL, Tokyo, Japan), and

the specimen surfaces were imaged using the bundled SEM Center/SMILE VIEW™ Lab software (v. 1.07/v. 1.0.2).

2.10.2. Fluorescence Microscopy

For fluorescence microscopy, the specimens were stained with an aqueous solution of acridine orange (0.1 mg/mL). A saturated solution of Sudan Black B in 70% ethanol was then applied to minimize background autofluorescence. After air-drying, the filter containing the biofilm was mounted on a microscope slide, sealed with a mixture of paraffin and petroleum jelly, and covered with a coverslip. Standard filter sets (sets 10 and 16, Carl Zeiss, Oberkochen, Germany) were used for microscopy.

2.11. Determination of Extracellular DNA Content by Fluorimetric Method

Each of the three biological replicates was analyzed in three technical replicates. In brief, the supernatant obtained after cell desorption from membrane filters, followed by centrifugation, was dispensed into the wells of a 96-well plate (100 µL per well) for fluorescence measurements. Immediately prior to measurement, 1 µL of an ethidium bromide solution (0.5 mg/mL in 5 mM Na_4EDTA) was added to each well. The plate was then incubated in the dark with shaking and scanned using a CLARIOstar Plus multimodal microplate reader (BMG LABTECH, Ortenberg, Baden-Württemberg, Germany) in fluorescence scanning mode at an excitation wavelength of 520 nm and an emission wavelength of 605 nm. Quantification was performed using a calibration curve constructed from standard DNA solutions prepared from lyophilized *E. coli* K12 DNA resuspended in buffer. The standard solutions covered concentrations of 1, 0.1, 0.01, 0.001 and 0.0001 mg/mL.

2.12. Determination of Protein Content Using Fluorescamine

For the fluorescence measurements, 75 µL of the sample and 25 µL of a 0.2 mg/mL fluorescamine solution (Abcam, Cambridge, UK) in dimethyl sulfoxide (DMSO) were added to each well of a 96-well plate according to the manufacturer's protocol (Fluorescein Protein Assay Kit, Abcam, ab324117). The plate was then incubated with shaking in the dark for 3 min at room temperature using a CLARIOstar Plus multimodal microplate reader (BMG LABTECH, Ortenberg, Baden-Württemberg, Germany). The fluorescence signal was measured at excitation and emission wavelengths of 380 and 470 nm, respectively. A calibration curve was constructed under the same conditions using a bovine serum albumin (BSA, 1 mg/mL, Sigma-Aldrich, St. Louis, MO, USA) standard at concentrations of 100, 10, 1, 0.1 and 0.01 µg/mL.

2.13. Calculation of the Specific Activity of Biofilm Cultures

To assess the synergistic effects of co-culturing bacteria, yeast, algae, and fungi in binary and multispecies biofilms, the specific activity index (*SAI*) was calculated according to Corte et al. [51]. This index reflects the relative change in the biomass or respiratory activity of the consortium compared to isolated monocultures. The specific metabolic capacity (SMC_m) of the monocultures was calculated using Equation (1):

$$SMC_m = \frac{OD_{INT(cul)}}{N_{cul}} \quad (1)$$

where SMC_m is the specific metabolic capacity of the monoculture, $OD_{INT(cul)}$ is the optical density of the formazan solution, and N_{cul} is the cell count in the biofilm.

The expected (additive) activity for composite biofilms OD_{exp} was calculated using Equation (2):

$$OD\,\mathrm{exp} = (SMC_{cul1} \times N_{cul1\_mix}) + (SMC_{cul2} \times N_{cul2\_mix}) \quad (2)$$

where OD_{exp} is the expected metabolic capacity; SMC_{cul1} and SMC_{cul2} are the specific metabolic capacities of monocultures 1 and 2, respectively; and N_{cul1_mix} and N_{cul2_mix} are the cell counts of cultures 1 and 2 in the mixed biofilm.

The final specific activity index (*SAI*) was calculated using Equation (3):

$$SAI = \frac{OD_{INT(mix)}}{OD_{exp}} \quad (3)$$

2.14. Statistical Analysis and Data Visualization

Preliminary data processing was conducted using Microsoft Excel 2019. Subsequent statistical analysis and data visualization were performed using Orange Data Mining (v. 3.38.1), supplemented with custom Python (v. 3.11) scripts. Data normality was assessed using both Excel and Orange. For non-normally distributed data, correlations were evaluated using Spearman's non-parametric rank correlation, with coefficients and *p*-values calculated via Orange workflows. Data for population dynamics, biomass, and extracellular matrix component concentrations are expressed as Mean ± Standard Error (SE) based on three biological replicates. No inferential hypothesis testing was performed for sequential time-point or between-treatment comparisons of these parameters; differences are described using strictly quantitative and descriptive terminology. To evaluate the synchronicity of temporal trends, Spearman rank correlation coefficients (r_s) were calculated across the pooled sequential data series (N = 12). The statistical significance of each r_s value was determined using the Student's t-distribution approximation, with differences considered statistically significant at $p < 0.05$. Mean values and standard errors of the mean (SEM) for time-series datasets were calculated in Excel based on both technical and biological replicates. Correlation coefficient heatmaps were generated in Orange using integrated Python scripts.

3. Results

3.1. Morphology and Phylogeny of the Strains

The experimental strains were identified to the genus level based on molecular markers and morphological characteristics (Figure 1).

The microalgae were assigned to the genus *Asterochloris*; their cells displayed typical morphological traits (Figure 1a) and aligned phylogenetically with related species (Figure S1). The bacterial isolate belonged to the genus *Gordonia* (Figure S2) and exhibited a cellular morphology characteristic of this taxon (Figure 1b). The fungal strain was identified as a member of the genus *Thelebolus* (Figure S3), with its mycelium demonstrating the distinct morphological features described for this genus by Mukhopadhyay et al. [52] (Figure 1c). Lastly, the yeast isolate was identified as belonging to the genus *Occultifur* (Figures 1d and S4).

3.2. Population Dynamics of Individual Groups in Monospecific Biofilms

Mono- and mixed cultures (biofilms) formed on nylon filters under identical conditions and within similar spatial limits. Visual assessment indicated that coverage of the filter surface area was approximately 50–70% (Figure 3).

With the exception of the yeast monoculture, cell counts and projected coverage increased throughout the experiment across all monospecific biofilms (Figures 4 and 5). The *Asterochloris* sp. microalgal population increased 65-fold (Figure 4c), while the *Thelebolus* sp. mycelial biomass increased threefold (Figure 4d). Bacterial cell counts increased by approximately half an order of magnitude, whereas the yeast cell count remained close to baseline (Figure 4a,b).

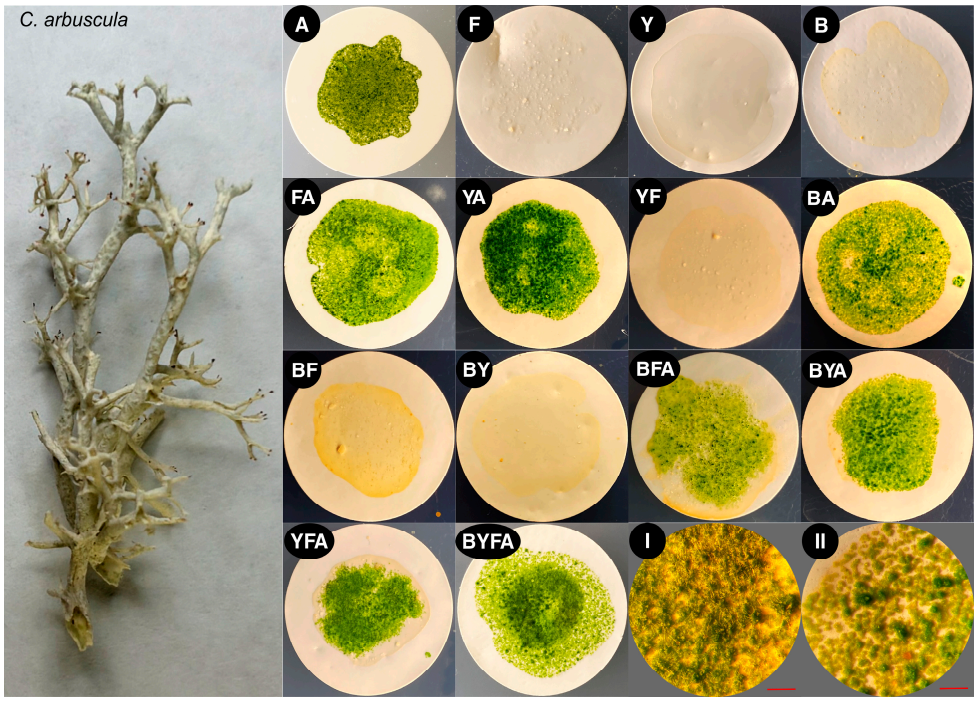


Figure 3. (Left) Thallus fragment of *Cladonia arbuscula*. (Remaining panels) Formation of mono- and mixed microbial biofilms on nylon filters (25 mm diameter) in various experimental combinations. Component designations: B—bacteria (*Gordonia* sp.), Y—yeasts (*Occultifur* sp.), F—fungi (*Thelebolus* sp.), and A—microalgae (*Asterochloris* sp.). Letter combinations indicate co-cultivation of the corresponding organisms. Images I and II were obtained using a stereomicroscope; the remaining images were captured using digital macro photography. (I)—binary biofilm FA; (II)—binary biofilm BA. Scale bar = 2 mm.

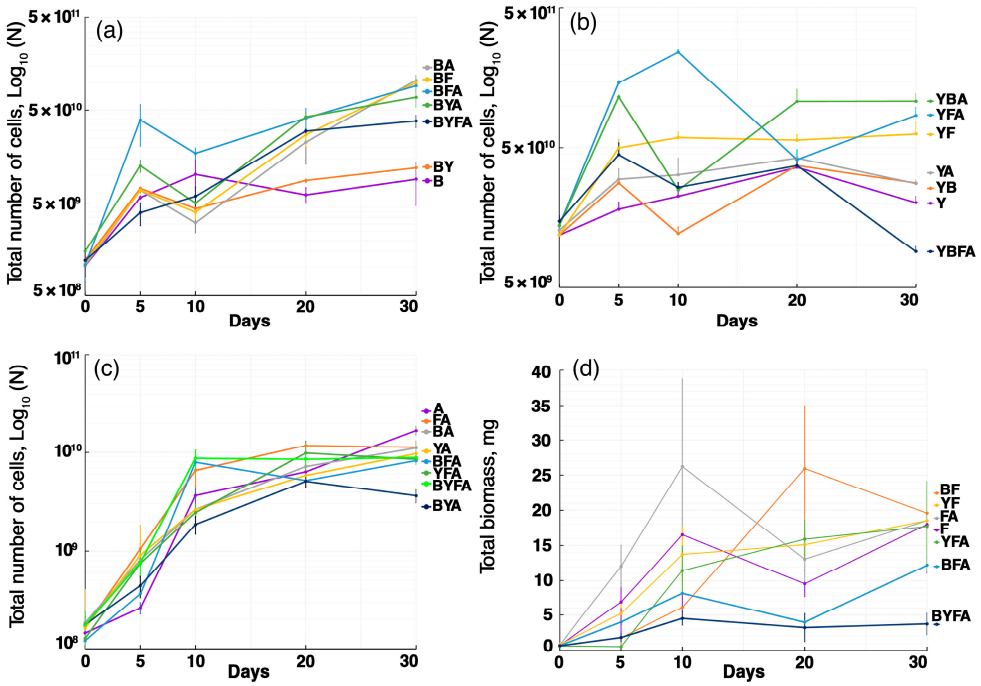


Figure 4. Dynamics of changes in the abundance of bacteria (**a**), yeasts (**b**), algae (**c**), and fungal biomass (mg) (**d**) over 30 days. Designations: B—bacteria (*Gordonia* sp.), Y—yeasts (*Occultifur* sp.), F—fungi (*Thelebolus* sp.), A—algae (*Asterochloris* sp.). Combinations of abbreviations indicate artificial consortia of these organisms. Data are presented as mean values ± standard error of the mean (SEM), $n = 3$.

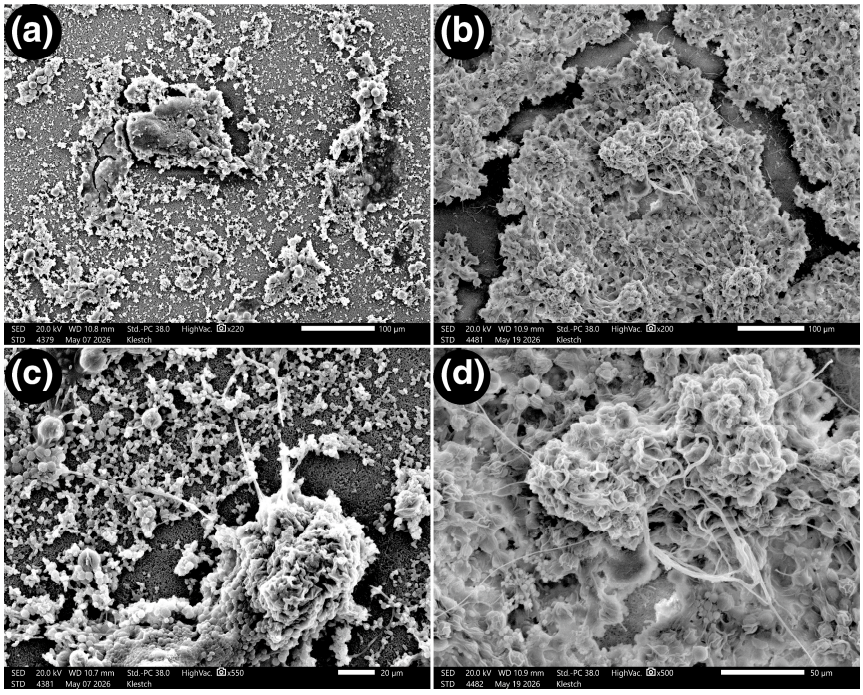


Figure 5. Micrographs of 4-component combined biofilms (*Gordonia* sp., *Occultifur* sp., *Thelebolus* sp., and *Asterochloris* sp.): (**a**,**c**)—5 days of exposure; (**b**,**d**)—30 days. Scanning electron microscopy. Magnification and scale bars: (**a**)—220×, 100 µm; (**b**)—200×, 100 µm; (**c**)—550×, 20 µm; (**d**)—500×, 50 µm.

Biofilm development was accompanied by the synthesis of an extracellular polymeric substance (EPS) matrix that encapsulated the cells (Figure S5a,b). In mature *Asterochloris* biofilms, young cells—specifically aplanospores—predominated (Figure S6). In mature *Thelebolus* sp. biofilms, the mycelium formed coiled rings, anastomoses, clusters and dense hyphal networks embedded within the EPS matrix (see Figure S7a). These fungi exhibited two distinct hyphal morphologies: thickened and thin (Figure S7b). The thickened hyphae were actively involved in matrix production, whereas the younger, actively growing hyphae colonized vacant zones on the membrane filter surface. Notably, the EPS matrix in *Asterochloris* monospecific biofilms was less pronounced than in biofilms containing *Thelebolus* sp. (Figure S5). In contrast, no significant population changes or matrix production were observed in the bacterial and yeast monocultures.

3.3. Population Dynamics of Individual Groups in Binary Biofilms

In binary biofilms, *Asterochloris* sp. counts dropped 5- to 6-fold compared to its monoculture (Figure 4c), while *Thelebolus* sp. biomass decreased slightly (Figure 4d). Conversely, co-culturing *Gordonia* sp. with either *Asterochloris* sp. or *Thelebolus* sp. stimulated bacterial growth 10-fold (Figure 4c). Additionally, *Gordonia* sp. induced a fourfold increase in *Thelebolus* sp. biomass (Figure 4d). SEM analysis confirmed this bacterial expansion in *Thelebolus* biofilms, showing *Gordonia* cells localized on the EPS matrix, directly on fungal hyphae (Figure S8a), and forming a dense mat on the filter membrane (Figure S8b). This suggests independent bacterial survival on low-glucose medium and potential utilization of fungal metabolites. In *Occultifur* sp. yeast binary combinations, only the mycelial fungi showed a slight biomass increase, while microalgal growth rates decreased, and other partner abundances remained at baseline levels. Crucially, the yeast population itself remained stable across all binary combinations throughout the 30-day incubation period (Figure 4b).

3.4. Population Dynamics of Individual Groups in Three- and Four-Component Biofilms

By day 30 in three-component biofilms, microalgal abundance peaked in the *Asterochloris–Gordonia–Thelebolus* consortium, while fungal biomass peaked in the *Asterochloris–Occultifur* pair (15-fold increase). *Gordonia* sp. counts rose markedly with *Asterochloris* sp. and *Occultifur* sp., though this microalgal stimulation was lower than in binary systems, suggesting fungi and yeast limited bacterial growth through competition. Conversely, yeast counts remained at baseline or dropped twofold. Microscopic analysis confirmed yeast cells localized exclusively on the filter surface and within the matrix without forming microcolonies on hyphae or microalgae (Figure S9). In the *Asterochloris–Thelebolus* binary control, microalgal growth was stimulated during the first 20 days before stabilizing (Figure 4). Fungal biomass significantly increased with bacteria or yeast during the first 20 days, peaking on day 10 when paired with microalgae. Concurrent bacterial and fungal presence slowed microalgal proliferation after day 10, or after day 20 when yeast was also added, highlighting heterotrophic dependence on the autotrophic partner. In four-component biofilms, *Gordonia* sp. abundance increased 10-fold, while *Asterochloris* sp. rose 11-fold, stabilizing at (8–9) $\times$ 10^9 cells after 10 days. Fungal biomass remained low near baseline values, contrasting with its 2.5-fold increase in monoculture. Yeast counts progressively declined 5-fold between days 5 and 30, with cells becoming virtually undetectable by SEM on day 30 (Figure S10a). Concurrently, abundant bacterial growth occurred on the outer microalgal layers and fungal hyphae walls, with microcolonies localizing predominantly on young microalgal aplanospores (Figure S10a).

3.5. Changes in the Concentration of Extracellular DNA and Proteins in Biofilms

Upon homogenization, it was hypothesized that all unbound extracellular DNA (exDNA) would be quantitatively transferred into a $Na_4EDTA \times 4H_2O$ solution (pH 8.0). Because a 5 mM sodium EDTA solution effectively chelates divalent metal cations, performing the extraction and subsequent handling of the supernatant at a low temperature (~4 °C on ice) ensured minimal DNA degradation. Furthermore, 5 mM $Na_4EDTA \times 4H_2O$ does not interfere with the intercalating binding of ethidium bromide (EtBr) to double-stranded DNA. Most water-soluble proteins also exhibit high solubility in a 5 mM $Na_4EDTA \times 4H_2O$ solution at pH 8.0 [53]. At pH 8.0, protein aggregation is minimized because the operational pH is sufficiently distant from the isoelectric points (pI) of the majority of these proteins, thereby maintaining electrostatic repulsion [54].

3.5.1. Changes in Extracellular DNA Concentration

In the monocultures, the concentration of exDNA ranged from 0.05 to 130 µg per total biofilm sample. In the *Asterochloris* sp. biofilm, the exDNA concentration increased progressively during incubation as cell counts rose, shifting from 0.74 to 131.64 µg, reflecting active culture growth and matrix development (Figure 6). In contrast, the exDNA concentration in the other monoculture variants changed only marginally.

In binary biofilms, microalgae were the primary source of exDNA (Figure 6a). The nucleic acid concentration increased by two orders of magnitude exclusively in co-cultures containing this autotrophic component. In contrast, the exDNA concentrations in binary biofilms composed strictly of heterotrophs (e.g., yeast, bacteria and fungi) remained comparable to those observed in their respective monocultures.

In the ternary biofilms, exDNA concentrations increased as the systems aged (Figure 6b). In the four-component biofilm comprising fungi, microalgae, bacteria and yeast, the exDNA concentration remained virtually unchanged during the first ten days of incubation. However, it increased by one order of magnitude by day 20 and by nearly three orders of magnitude by day 30 (Figure 6b).

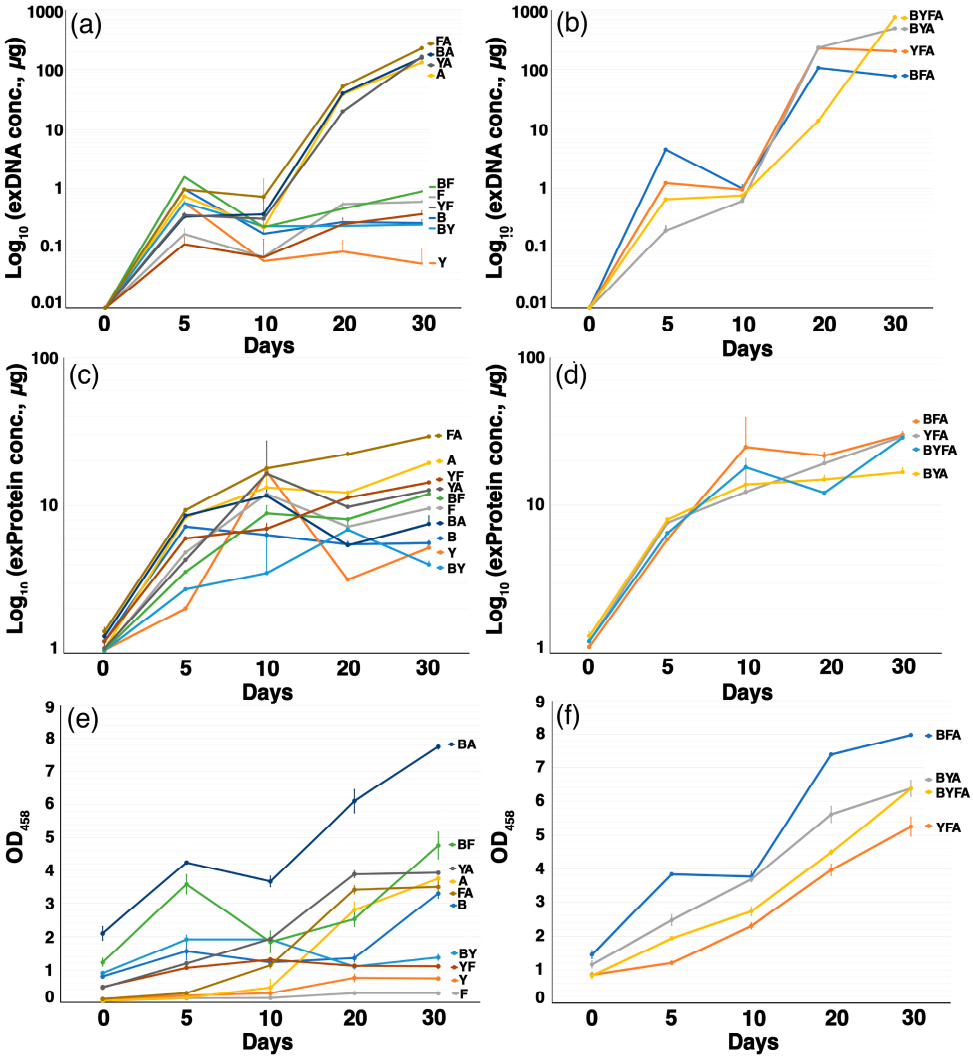


Figure 6. Dynamics of extracellular DNA concentration (**a**,**b**), extracellular protein concentration (**c**,**d**), and optical density (OD_{458}) of formazan solution (**e**,**f**) during 30 days of incubation of monocultures and binary biofilms (**a**,**c**,**e**), as well as three- and four-component consortia (**b**,**d**,**f**). Designations: B—bacteria (*Gordonia* sp.), Y—yeasts (*Occultifur* sp.), F—fungi (*Thelebolus* sp.), A—algae (*Asterochloris* sp.). Combinations of abbreviations indicate artificial consortia of these organisms. Data are presented as mean values ± standard error of the mean (SEM), $n = 3$.

3.5.2. Changes in Extracellular Protein Concentration

Extracellular proteins (exProt) and exDNA are integral structural components of the biofilm matrix. However, proteins secreted by heterotrophic organisms often perform vital enzymatic functions beyond this structural role.

A distinct increase in extracellular protein concentration was observed in the monocultures on day 10 of incubation for both the fungal and yeast biofilms (Figure 6c: *F*, *Y*). Meanwhile, protein concentrations decreased noticeably in binary biofilms containing yeast and bacteria, and to a lesser extent in those containing the mycelial fungus. As with the trends observed for exDNA, the maximum absolute increase in extracellular protein concentration occurred in the *Asterochloris* sp. monoculture. In this microalgal biofilm, proteins were actively released into the extracellular medium between days 0 and 20 of the experiment (Figure 6c: *A*), whereas a sharp increase in exDNA secretion occurred after day 10 (Figure 6a). By contrast, extracellular proteins in bacterial monocultures remained at consistently low concentrations throughout the experiment (Figure 6c: *B*).

In binary biofilms, the fungus–microalgae complex dominated extracellular protein synthesis, with concentrations increasing threefold between days 0 and 30 (Figure 6c: *FA*). Notably, the peak in protein production observed on day 10 persisted in the binary biofilm containing both yeast and microalgae, mirroring the pattern seen in the single-species yeast culture (Figure 6c: *Y*, *YA*).

At the same time, the concentration of extracellular proteins increased gradually in binary biofilms based on fungi (Figure 6c: *BF*, *YF*), but decreased in *BA* and *BY* systems (Figure 6c). All three-component biofilms exhibited an upward trend in protein levels. While the bacteria–yeast–microalgae consortium exhibited only a marginal increase, the other multi-species combinations matched the accumulation kinetics and final concentrations after 30 days of the mycelial fungus–microalgae binary culture (Figure 6d). The four-component biofilms followed this overall accumulation trend, except for a sharp decline on day 20. This fluctuation mirrored that observed in yeast-containing biofilms, where protein concentrations dropped from an initial 16–18 μg to 3 μg (yeast monoculture), 9 μg (binary microalgal co-culture) and 12 μg (four-component biofilm). In three-component biofilms, these fluctuations were absent or masked. These findings suggest that microalgae primarily drive extracellular protein accumulation. However, unlike exDNA dynamics, which are modulated by bacteria, yeast regulates secretion and stabilizes the extracellular protein pool. The expansion of the matrix pool may be further driven by yeast autolysis induced by nutrient deprivation [55].

3.6. Level of Metabolic Potential in Biofilms

As the experimental design involved evaluating metabolic performance in the presence of exogenous energy sources (liquid FA+ medium), the findings from these assays reflect the potential metabolic activity of the systems. The rate of iodonitrotetrazolium (INT) reduction varied depending on the specific community composition and culture age of both the monocultures and multi-species biofilms (Figure 6e: *F*). Consortia combining bacterial and microalgal components consistently exhibited the highest potential activity. Accordingly, binary and ternary cultures featuring this bacterium–microalgae pairing achieved maximum metabolic outputs. Conversely, the *Gordonia–Occultifur* (*BY*) and *Occultifur–Thelebolus* (*YF*) binary systems demonstrated the lowest overall activity, mirroring the baseline profiles of the yeast and fungal monocultures. The metabolic dynamics of the *Gordonia–Thelebolus* (*BF*) binary system were comparable to those of the *Gordonia* sp. monoculture (Figure 6e): both exhibited a gradual decline in activity over time. This implies that the bacterial component predominantly contributed to the overall metabolic output of this pairing.

The lowest metabolic levels were observed in consortia that consisted entirely of heterotrophic organisms. In these systems, intense substrate competition likely suppressed metabolic performance overall against a backdrop of nutrient depletion from external sources. In contrast, metabolic activity remained high in three-component consortia, driven primarily by the bacterial and microalgal components. In the four-component biofilm, metabolic activity increased proportionally with biofilm maturity (Figure 6f). This progressive increase was strongly correlated with the expansion of the autotrophic component (*Asterochloris* sp.), which is the system's primary producer—a finding supported by both population abundance data (Figure 4) and scanning electron microscopy observations (Figure 5).

3.7. Specific Activity of Components in Composite Biofilms

To test the hypothesis that biofilm metabolic performance depends directly on the abundance or biomass of its individual components, the specific activity index *SAI* was

calculated using the equations detailed in Section 2.13. An index value greater than 1 indicates metabolic synergy within the system, whereas a value less than 1 denotes metabolic inhibition.

Assessment of the *SAI index* revealed distinct phases of both synergistic activation and metabolic suppression across the studied consortia. These phases varied markedly depending on biofilm composition and incubation period (Figures 7 and S11). A sharp peak in the *SAI* parameter on day 10 was characteristic of the *BY* (2.21), *BF* (2.55) and *BA* (2.40) binary systems, indicating a pronounced respiratory burst during which the cells' respiration rates accelerated. By days 20–30, however, these indices had fallen below 1. In the case of the *BF* and *BA* binary biofilms, they had dropped to critically low levels (0.09 and 0.17, respectively). This sharp decline indicates a transition into a phase of profound metabolic inhibition, suggesting a rapid transition of the cells into a zero-growth phase.

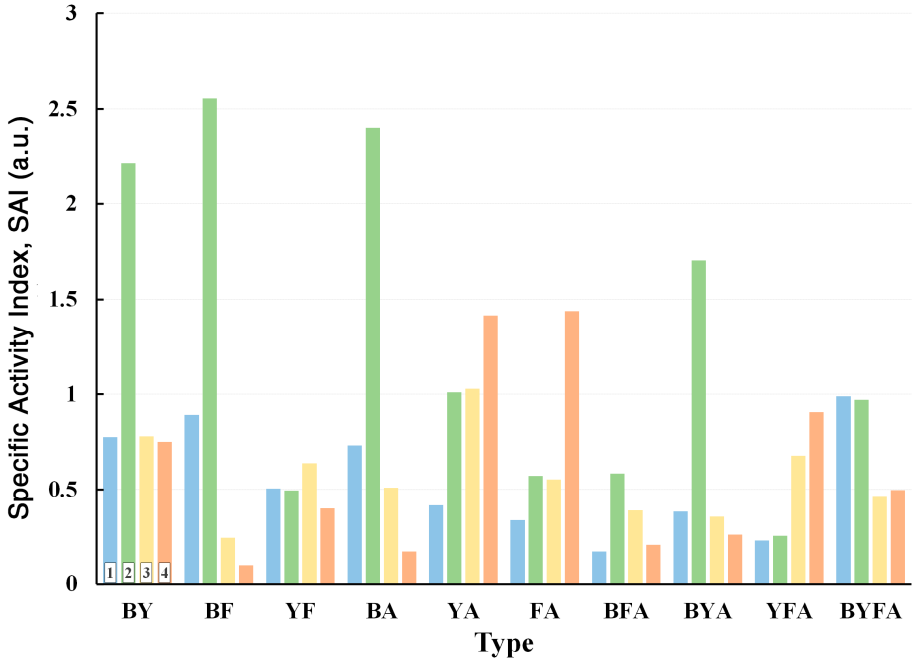


Figure 7. Specific activity index (*SAI*) of binary, three-, and four-component biofilms depending on the consortium composition and incubation time. Designations: B—bacteria (*Gordonia* sp.), Y—yeasts (*Occultifur* sp.), F—fungi (*Thelebolus* sp.), A—algae (*Asterochloris* sp.). Letter combinations indicate artificial consortia of these organisms. Sampling points: 1 (blue)—day 5; 2 (green)—day 10; 3 (yellow)—day 20; 4 (orange)—day 30.

Given the high baseline activity of *Gordonia* sp., these synergistic effects are primarily associated with a substantial increase in metabolic output by the bacterial component. This is supported by contrasting behaviors observed in *YA* and *FA* binary biofilms. While these two systems remained stable on days 5 and 10 of the experiment, they both reached peak activity by day 30 (*SAI* > 1.4), signalling a prolonged synergistic effect coupled with an increase in microalgal cell counts. In contrast, within the strictly heterotrophic *YF* system, the index fluctuated within a narrow, stable range below the reference baseline (0.40–0.63) throughout the experiment. This indicates persistent metabolic suppression in the absence of sharp ecological or metabolic shifts at the cellular level. In the three-component consortia (*BFA*, *BYA* and *YFA*), the specific activity of the cells generally decreased over time. However, a distinct stabilizing effect was noted specifically for the *BYA* consortium. Conversely, metabolic inhibition in the *BFA* system was the most pronounced of all the studied biofilms, remaining far below 1.

The delayed shift observed in the *YFA* biofilm was characterized by a smooth, linear increase in activity. Starting from a highly inhibited state of 0.22, it rose towards the additive threshold of 0.90 by the end of the experiment. Ultimately, the combination of these population factors minimized the initial antagonistic effects. Thus, while high, oscillating specific activity is fundamentally driven by bacterial dynamics, a smooth, gradual increase in this parameter is closely tied to microalgal population growth and the strengthening of physical interactions between distinct components as overall biofilm density increases (Figure 5).

An early plateau of stable activity near the additive threshold was observed within the four-component biofilm. Unlike the binary and ternary systems, the *BYFA* consortium exhibited consistently stable baseline activity during the initial stages, achieving values of 0.98 on day 5 and 0.97 on day 10. However, by day 20, a sharp metabolic transition occurred, during which the index decreased twofold to 0.46, indicating a shift towards metabolic inhibition. This sudden drop suggests an ecological state transition, wherein the increased structural complexity and specific density of the ageing biofilm trigger metabolic restructuring, driving the community towards a more energy-efficient, yet stable, metabolic state.

3.8. Synergistic Effects in Mixed Biofilms

To evaluate the extent to which multi-species biofilms differed from single-species controls in terms of exDNA secretion, protein release and potential metabolic activity, the values for these parameters were summed for individual monocultures and then compared with the values obtained from the mixed consortia. The final values were then expressed as a percentage of the combined baseline sum of exDNA and protein concentrations, as well as the optical density of the formazan solution, in the monocultures (Figure 8).

The release of exDNA and proteins into the extracellular space is an indicator of two processes: passive cell autolysis, where intracellular contents are released into the surrounding medium, and directed secretion, which establishes intercellular communication and deploys functional extracellular enzymes. In most binary biofilms, the cumulative concentration of exDNA resulting from the two species was lower than the total sum of exDNA calculated from the corresponding monospecific controls (Figure 8a,b). A significant synergistic effect was exclusively observed on day 10 within the *FA* binary biofilm, coinciding with the period of active mycelial growth and microalgal reproduction. Conversely, on days 20 and 30, this synergistic trend decreased as spatial constraints within the matrix became limiting.

A weak synergistic effect was observed in the *BF* biofilm on day 5, which was likely driven by initial matrix development and the adaptation of the components to spatial co-localization. Within the three-component biofilms *YFA* and *BYA*, the cumulative exDNA concentration rose progressively from day 5 to day 30 (Figure 8b), ultimately exceeding several hundred percent relative to the single-species controls. Indeed, across the majority of the three-component biofilms, the final exDNA concentrations significantly surpassed the 100% baseline, with the sole exception of the *BFA* biofilm on day 30.

In contrast, within the four-component biofilms, the cumulative concentration only slightly exceeded the monoculture sum on days 10 and 30 of the experiment. This trend reflects a diminished structural role for exDNA in matrix consolidation, likely due to the extensive production of alternative EPS by the fungal mycelium and microalgae (Figure 8b). Consequently, the synergistic accumulation of exDNA is primarily characteristic of three-component systems where heterotrophic cultures comprise either the entire community or at least two-thirds of the total species pool.

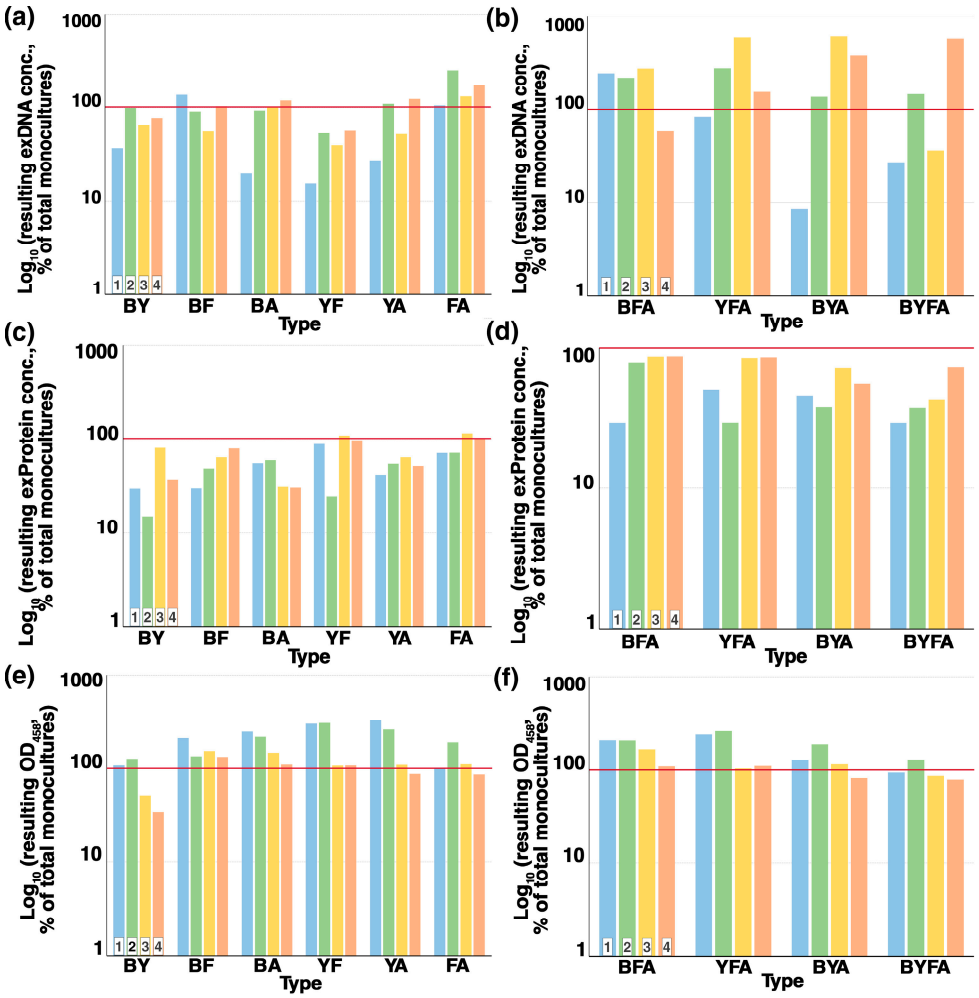


Figure 8. Evaluation of synergism in binary (**a**,**c**,**e**) and multi-component (**b**,**d**,**f**) biofilms based on extracellular DNA concentration (**a**,**b**), extracellular protein concentration (**c**,**d**), and optical density (OD_{458}) of formazan solution (**e**,**f**) during 30 days of incubation. Data are presented on a logarithmic scale as a percentage of the total indicators of the respective monocultures. The red horizontal line indicates the 100% baseline (theoretical additive effect). Numbers 1–4 indicate sampling times: 1 (blue)—day 5; 2 (green)—day 10; 3 (yellow)—day 20; 4 (orange)—day 30. Designations: B—bacteria (*Gordonia* sp.), Y—yeasts (*Occultifur* sp.), F—fungi (*Thelebolus* sp.), A—algae (*Asterochloris* sp.). Combinations of abbreviations indicate artificial consortia of these organisms.

This trend is likely driven by elevated autolysis rates in these purely heterotrophic systems, which lack autotrophic primary producers. This signifies accelerated cell mortality due to nutrient starvation. Extracellular proteins are also critical components of the biofilm matrix. As well as playing a structural role, the matrix and intercellular spaces contain actively secreted peptides and functional enzymes, as well as proteins and amino acids released from cells undergoing autolysis. In virtually all multi-species combinations, no synergistic effect was observed; the cumulative concentration of the resulting protein was lower than the theoretical sum calculated from the individual monocultures. A synergistic increase in protein concentration was exclusively observed in select mature biofilms on days 20 and 30 (Figure 8c,d). Specifically, this effect was noted in the *YF* binary co-cultures on day 20 (albeit weakly), and in the *BYA* ternary biofilms on days 20 and 30. These results closely replicate the synergistic trends observed for exDNA.

Metabolic synergy was most evident on days 5 and 10 of the biofilm incubation period, as determined by the rate of formazan reduction (Figure 8e,f). Overall, the metabolic activity of the multi-species biofilms exceeded that of the individual monocultures by

120–300%, with this effect being particularly pronounced in binary systems. Exceptions to this trend included two binary biofilms (*BY* and *FA*) and the four-component biofilm. In these consortia, the level of metabolic activity remained below 100% of the sum of the monocultures on day 5, declining further on days 20 and 30. As the biofilms matured, the level of cumulative metabolic activity gradually approached or fell below the baseline total activity of the individual monocultures (Figure 8e,f).

3.9. Magnitude of Change in Measured Parameters

To evaluate the overall dynamics of biofilm development, the fold change of each parameter was calculated by dividing the final value on day 30 by the corresponding baseline value on day 5 (Table 1). The greatest increase in exDNA concentration was observed in multi-species biofilms containing *Asterochloris* sp., while the lowest fold changes for this parameter were recorded in *Thelebolus* sp. monocultures, *YF* binary co-cultures and *BFA* three-component biofilms. Meanwhile, exDNA concentrations declined over time in heterotrophic monocultures and binary biofilms that included the bacterial component.

Table 1. The fold change in the optical density of the formazan extract (F-OD_{450}), the concentration of extracellular DNA (exDNA) and extracellular protein (exProt) on day 30 relative to day 5.

Cultures	F-OD_{458}	exDNA	exProt
B	2.1	0.3	0.8
Y	3.4	0.1	8.1
F	2.1	3.5	2
A	24.7	177	2.3
BY	0.7	0.4	1.5
BF	1.3	0.6	3.3
BA	1.8	468	0.9
YF	1	3.2	2.4
YA	3.3	457.4	2.9
FA	12	235	3.2
BFA	2.1	16.8	5.1
YFA	4.3	162.6	3.8
BYA	2.6	2541.3	2.1
BYFA	3.3	1150.4	4.4

The greatest increase in metabolic activity was observed in the *Asterochloris* sp. monoculture and in its binary association with *Thelebolus* sp. By contrast, the least significant increase in activity, or even a decrease, was observed in the heterotrophic biofilms *BY*, *BF* and *YF*. Furthermore, within biofilms containing a bacterial component, the fold change in exProt concentration was minimal; however, the presence of yeast and filamentous fungi significantly contributed to an increase in this parameter. The most significant increase in extracellular protein concentration was observed in the yeast monoculture. Given the highly stable cell population size, this trend likely indicates accelerated cell mortality induced by nutrient starvation and subsequent autolysis.

3.10. Correlations Between Abundance, exDNA Concentration, exProtein Concentration, and Potential Metabolic Activity

The dynamics of changes in the abundance parameters of unicellular microorganisms and the mycelial biomass of filamentous fungi were compared against the cumulative metabolic activity of the biofilms, as well as their respective extracellular DNA and protein concentrations. It is important to note that, since these variables change simultaneously over the course of exposure, the observed correlations reflect parallel temporal trends and do not demonstrate direct causality. To evaluate the synchronization of these parameters'

temporal trends across the studied microbial groups and their consortia, a Spearman rank correlation analysis was performed using the pooled replicates across all sequential time points (N = 12). The significance of each association was assessed based on the corresponding p-value (see Figures 9 and 10). Initial evaluations focused on comparing the correlations among the concentrations of exDNA, exProt, and formazan (Figure 9).

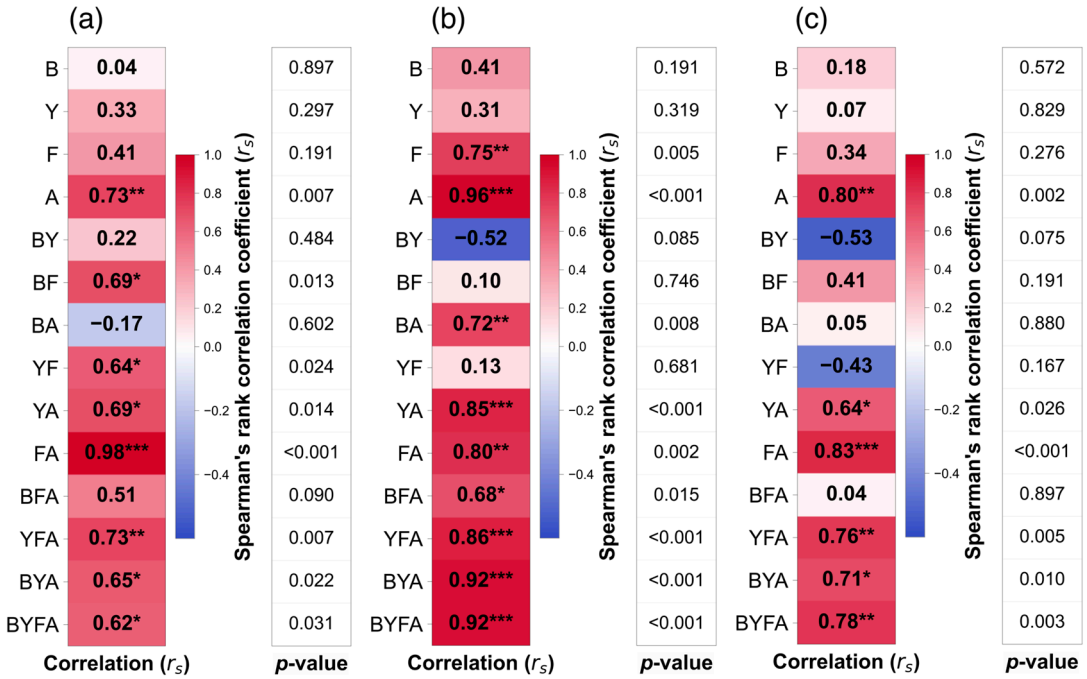


Figure 9. Heatmaps of Spearman rank correlation coefficients (r_s) and corresponding p-values reflecting the relationship between: (**a**) extracellular DNA and extracellular protein concentrations; (**b**) extracellular DNA and formazan concentrations; and (**c**) extracellular protein and formazan concentrations. Designations: B—bacteria (*Gordonia* sp.), Y—yeasts (*Occultifur* sp.), F—fungi (*Thelebolus* sp.), A—algae (*Asterochloris* sp.). Letter combinations indicate artificial consortia of these organisms. Asterisks indicate statistically significant correlations: * $p < 0.05$, ** $p < 0.01$, *** $p < 0.001$. The correlation was calculated across the pooled sequential series (N = 12) to assess the synchronicity of temporal trends.

3.10.1. Covariation Trends of exDNA and exProt Concentrations

Analysis of the parallel temporal trends between exDNA and exProt concentrations (based on pooled replicates across the exposure period, N = 12) revealed highly diverse patterns of synchronous co-alteration, ranging from weak negative associations to strong positive ones (Figure 9a). The strongest synchrony was observed in the microalgae–fungus consortium (*FA*), reaching a value of (r_s = 0.98, $p < 0.001$). High and statistically significant correlation coefficients, indicating tightly matched temporal dynamics, were also characteristic of both the microalgae monoculture (*A*, r_s = 0.73, $p < 0.01$) and the three-component consortium comprising yeast, fungi, and microalgae (*YFA*, r_s = 0.73, $p < 0.01$).

Additionally, consistent positive dynamics were noted for the *BF* and *YA* (r_s = 0.69, $p < 0.05$ for both) consortia, indicating a high degree of coordinated temporal shifts within these specific combinations. In contrast, the bacterial control culture (*B*) exhibited a nearly neutral and statistically non-significant correlation (r_s = 0.04, $p > 0.05$).

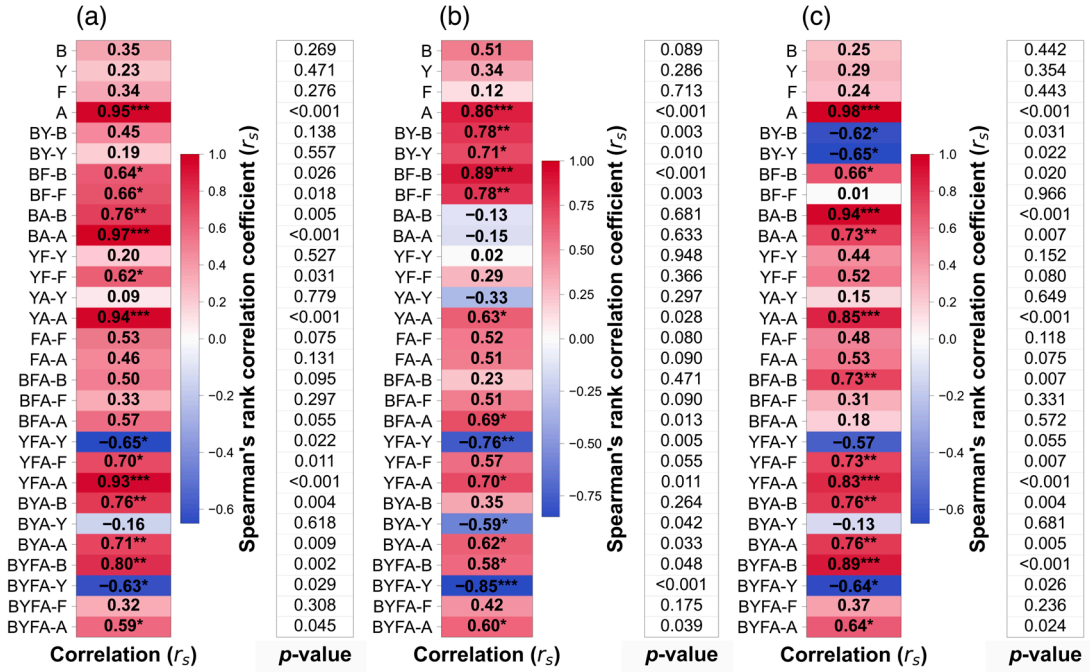


Figure 10. Heatmaps of Spearman rank correlation coefficients (r_s) and corresponding *p*-values reflecting the relationship between the abundance or biomass of microorganisms and: (**a**) extracellular DNA concentrations; (**b**) extracellular protein concentrations; and (**c**) formazan concentrations. Designations: B—bacteria (*Gordonia* sp.), Y—yeasts (*Occultifur* sp.), F—fungi (*Thelebolus* sp.), A—algae (*Asterochloris* sp.). Letter combinations indicate artificial consortia of these organisms. Asterisks indicate statistically significant correlations: * $p < 0.05$, ** $p < 0.01$, *** $p < 0.001$. The correlation was calculated across the pooled sequential series ($N = 12$) to assess the synchronicity of temporal trends.

3.10.2. Covariation Trends of Potential Metabolic Activity and exDNA Concentration

Analysis of the correlation between the potential activity parameter and exDNA concentration revealed highly significant, strong-to-extremely-strong positive correlations for the two key eukaryotic components within their respective monospecific biofilms (Figure 9b). Within biofilms formed by *Asterochloris* sp., the highest correlation was observed between exDNA concentration and potential activity ($r_s = 0.96$, $p < 0.001$), reflecting a tight coordination between extracellular matrix accumulation and the metabolic dynamics of the photobiont. Similarly, a strong correlation was found between these parameters in the mycelial fungal monoculture ($r_s = 0.75$, $p = 0.005$). In contrast, when analyzed in isolation, no statistically significant correlations between exDNA concentration and metabolic activity were detected for the prokaryotic and yeast components (bacteria: $r_s = 0.41$, $p = 0.191$; yeast: $r_s = 0.31$, $p = 0.319$).

When evaluating interspecies pairwise interactions, the correlation landscape shifted significantly compared to isolated monocultures. Strong and very strong positive correlations were identified for the *YA* (*Occultifur–Asterochloris*) and *FA* (*Thelebolus–Asterochloris*) binary systems ($r_s = 0.85$, $p < 0.001$ and $r_s = 0.80$, $p = 0.002$, respectively). These findings highlight a highly synchronized co-development pattern within these co-cultures, suggesting that the presence of the microalgae may play a key role in coordinating the growth dynamics of both the fungal and yeast components.

When analyzing the relationship between exDNA concentration and potential activity, the binary pairs exhibited varying trends. The *BA* pair showed a strong positive correlation ($r_s = 0.72$, $p = 0.008$), while the *BF* and *YF* pairs were not significant ($p > 0.05$). In contrast, the *BY* pair demonstrated a borderline negative trend ($r_s = -0.52$, $p = 0.085$), suggesting a potential tendency towards antagonism. Notably, integrating these components into

multi-species consortia resulted in highly synchronized temporal dynamics. Strong to extremely strong positive correlations were observed across all complex systems, including the ternary consortia *BFA* (r_s = 0.68, p = 0.015), *YFA* (r_s = 0.86, $p < 0.001$) and *BYA* (r_s = 0.92, $p < 0.001$). This resulted in maximum synchrony within the four-component *BYFA* consortium (r_s = 0.92, $p < 0.001$).

3.10.3. Covariation Trends of Potential Metabolic Activity and exProt Concentration

When evaluating exProt concentration against potential metabolic activity, a strong positive correlation was found exclusively for the microalgae monoculture (r_s = 0.80, p = 0.002), while other monospecies biofilms showed non-significant trends ($p > 0.05$) (Figure 9c). Among pairwise systems, the photobiont-containing consortia exhibited closely coordinated temporal dynamics, with a very strong positive correlation in the *FA* binary biofilm (r_s = 0.83, $p < 0.001$) and a moderate one in the *YA* system (r_s = 0.64, p = 0.026). In contrast, the *BF* and *BA* pairs were non-significant ($p > 0.05$), and the negative coefficients for the *YF* ($r_s = -0.43$) and *BY* ($r_s = -0.53$, p = 0.075) pairs did not reach statistical significance, though the latter maintained a potential tendency toward antagonism.

Grouping these components into multi-species consortia revealed a clear pattern: statistical significance was exclusively maintained in setups where microalgae were present. Specifically, strong positive correlations were observed in the *YFA* (r_s = 0.76, p = 0.005) and *BYA* (r_s = 0.71, p = 0.010) complexes. In contrast, correlations in complexes lacking the microalgae component were entirely non-significant. Finally, the comprehensive four-component symbiotic consortium (*BYFA*) exhibited a robust positive correlation between these parameters (r_s = 0.78, p = 0.003).

3.11. Relationship Between Population Size/Biomass and exDNA Concentration

The association between population size or biomass and exDNA concentration was positive and reliable only when microalgae or fungi were present (Figure 10a). Although yeast abundance showed a weak correlation under most conditions, it exhibited a distinct and statistically significant negative correlation within the *YFA* and *BYFA* multi-species complexes. This divergence may reflect intense interspecific competition or a shift in population dynamics. During the development of the *YFA* complex biofilm, where fungi and microalgae proliferated actively, the yeast population may have experienced growth suppression. Consequently, a decline in yeast abundance occurred against the backdrop of an expanding total exDNA pool driven by the other co-existing organisms, which could explain the observed negative correlation trend.

When evaluated in isolation within monospecific biofilms, there were weak correlations between abundance/biomass and exDNA concentration for both *Gordonia* sp. and *Thelebolus* sp. (r_s = 0.35 for bacteria; r_s = 0.34 for fungi). However, when co-cultured in pairs, their correlation coefficients increased markedly. Within the *BF* binary biofilm, the correlation became moderately strong for both species (r_s = 0.64 for *Gordonia* sp. and r_s = 0.66 for *Thelebolus* sp.). Similarly, in the *BA* pair, the bacterial component demonstrated a strong and reliable correlation (r_s = 0.76) (Figure 10a). These trends collectively suggest that co-cultivation, particularly with microalgae or in bacteria–fungi pairings, leads to a more coordinated pattern of population growth and structural development. Consequently, the accumulation of exDNA within the matrix becomes tightly coupled with biomass progression, resulting in a highly predictable, synchronous temporal trend between cell abundance and extracellular matrix formation.

3.12. Relationship Between Extracellular Protein Concentration and Cell Number or Mycelial Biomass

As with the trends observed for exDNA, a strong positive correlation was noted exclusively within the monospecies *Asterochloris* sp. biofilms between extracellular protein concentration and cell abundance (r_s = 0.86, $p < 0.001$; Figure 10b). In simple binary systems, the strongest and most reliable positive correlations between cell counts and protein levels were observed in the *BY* (*Gordonia–Occultifur*) pair (r_s = 0.78 for bacteria and 0.71 for yeast) and the *BF* (*Gordonia–Thelebolus*) pair (r_s = 0.89 for bacteria and 0.78 for fungi). In contrast, a significant shift was observed in the *BA* (*Gordonia–Asterochloris*) pair, where the correlation decreased to almost zero or became slightly negative (r_s = −0.13 for *Gordonia* sp. and −0.15 for *Asterochloris* sp.). This effect most likely reflects a dynamic equilibrium between extracellular protein consumption and active cell lysis: in an actively growing biofilm, the processes of protein secretion and subsequent utilization appear to be closely balanced. Mirroring the exDNA dynamics, yeast abundance in multi-component systems correlated negatively with extracellular protein concentrations, dropping to r_s = −0.76 in *YFA*, −0.59 in *BYA*, and −0.85 in *BYFA* (Figure 10b), which suggests divergent temporal trajectories for the yeast population within complex consortia. In contrast, the microalgal component exhibited a steady, statistically significant positive correlation across all multi-species systems (*YA*, *YFA*, *BFA*, *BYA*, and *BYFA*), with r_s values consistently ranging from 0.60 to 0.70 ($p < 0.05$). This indicates that microalgal population growth was highly synchronized with an increase in extracellular protein concentrations, reflecting their tightly coupled co-accumulation during the development of a stable biofilm architecture.

3.13. Relationship Between Dehydrogenase/Respiratory Potential Activity and Microbial Abundance or Biomass

Potential metabolic activity consistently showed strong positive correlations with microalgal abundance (r_s = 0.64–0.98) across nearly all combinations, except for the *BFA* consortium (r_s = 0.18), and with bacterial abundance across all complex consortia (*BA*, *BFA*, *BYA*, and *BYFA*); (r_s = 0.73–0.94, Figure 10c). These highly synchronized trends reflect the dominant contribution of the bacterial and microalgal components to the cumulative metabolic activity of the aging biofilm. Conversely, the yeast component exhibited a complete decoupling from metabolic activity in the presence of bacteria, showing significant negative correlations in the *BY* co-culture (r_s = −0.65) and the four-component *BYFA* system (r_s = −0.64), which suggests a decline in viable yeast presence as more competitive partners expand. Meanwhile, the filamentous fungus showed no statistically significant correlations between potential metabolic activity and biomass across any multi-species systems ($p > 0.05$), indicating that changes in fungal biomass did not run parallel to the cumulative metabolic shifts during biofilm maturation.

4. Discussion

The results of this study are consistent with the well-established chronological progression of biofilm development, which includes initial attachment, maturation and subsequent senescence, as previously described for numerous multi-species microbial systems [56]. However, our data also revealed several distinct patterns that are governed by the specific community composition and the temporal dynamics of biofilm growth. A key finding of this study is the dominance of the autotrophic component as the primary biomass producer in the absence of an organic substrate, alongside the severely restricted proliferation of heterotrophic microorganisms. Microalgae drive the primary synthesis of organic matter and secrete extracellular metabolites, such as exDNA, proteins, and polysaccharides, into the extracellular matrix of the forming consortium. This phenomenon occurs as a result

of routine metabolic activity [57,58] and presumably during the release of aplanospores from the maternal cell wall—a mechanism that is poorly documented in the literature. In theory, all genetic material and cytoplasmic nucleic acids from the microalgal mother cell (aplanosporangium) should be transferred to the daughter cells (aplanospores). However, there is currently no data available to confirm or refute the release of free nucleic acids upon rupture of the aplanosporangium cell wall. Furthermore, pronounced metabolic activity and significant exDNA accumulation were characteristically associated with the presence of bacteria. These prokaryotes were evidently the second most influential component within the biofilms, stabilising the processes of population growth and structural consolidation in complex systems in several instances.

Actinobacteria of the genus *Gordonia* are highly adapted to survive in adverse environmental conditions [59]. Their presence in the thalli of *Cladonia arbuscula* may be due to their resistance to lichen acids and their ability to remain viable in conditions of moisture deficiency and a lack of mineral nutrients and easily digestible organic matter. The high metabolic activity exhibited by *Gordonia* sp. in both monocultures and complex biofilms may be due to their active involvement in matrix synthesis and architectural regulation.

The filamentous fungus *Thelebolus* sp. demonstrated pronounced trophic plasticity and morphological adaptation across the various stages of biofilm development due to its distinct physiological traits. In monoculture, it actively established an interconnected mycelial network despite the extreme scarcity of organic substrates (using a medium containing only 50 mg/L glucose). Within multi-species biofilms, *Thelebolus* sp. presumably functioned as the primary producer of the extracellular polymeric substance (EPS) matrix. This matrix is clearly visible in scanning electron micrographs as a dense, sheet-like structure that anchors the embedded mycelium alongside the cells of the other biofilm components, such as microalgae, bacteria and yeast. However, the absolute levels of biomass, extracellular protein and exDNA production, as well as the respiratory potential, generated by *Thelebolus* sp. were substantially lower than those recorded for the microalgal and bacterial components, dropping to thresholds comparable to the yeast baseline.

The synergistic effects of exDNA production were more pronounced in three-component systems during the later stages of biofilm development. Conversely, metabolic activity increased more significantly within binary biofilms and ternary consortia during the early phases of colonization. There were virtually no emergent effects in extracellular protein production across all system configurations studied. This lack of synergy is probably due to the fact that the extracellular protein pool is a highly dynamic component that predominantly serves trophic and regulatory functions rather than playing a primary structural role [6]. The origin of extracellular DNA in the studied model biofilms is still unclear. It is most likely that active secretion and passive diffusion via autolysis occur simultaneously. However, it is currently not possible to determine the exact source of this DNA within the proposed experimental model and the methods used.

The morphological, structural and metabolic patterns of biofilm configuration within the investigated consortia revealed a dual development model. Firstly, the fungus *Thelebolus* sp. establishes a physical mycelial network, supplemented by its EPS matrix. Secondly, *Asterochloris* sp. microalgae are steadily expanded within this matrix. These microalgae generate substantial quantities of exDNA as population numbers rise and the biofilm matures. Simultaneously, the system features a dynamically expanding bacterial population characterized by high metabolic rates and intensive division kinetics, whereas the yeast component displays minimal reproductive and metabolic activity.

The manifestation of emergent effects within these multi-species biofilms is most likely due to cultivation on a nutrient-deprived medium forcing the establishment of stable syntrophic and spatial relationships within binary and more complex consortia. This aligns

with previously documented biofilm systems [32,60–62]. However, there are distinct differences between strictly heterotrophic consortia and those containing an autotrophic partner. High metabolic activity and the associated accumulation of exDNA were exclusively characteristic of systems featuring microalgae, whereas these indicators remained low in purely heterotrophic communities. Conversely, extracellular protein production profiles were comparable across nearly all studied setups, although a positive and statistically robust influence of the autotrophic partner on protein secretion kinetics could still be observed. Once again, it is important to emphasize that all biofilms containing microalgae exhibited a significant increase in extracellular DNA. In contrast, all heterotrophic biofilms (i.e., those without microalgae) exhibited only a slight increase.

Thus, under carbohydrate-deficient conditions, the phototrophic component dominates biofilm development and establishes a stable metabolic foundation: it constructs an exDNA-based framework, secretes a moderate baseline of extracellular proteins, and maintains a high respiratory rate. Here, extracellular DNA functions as a structural polymer that, together with proteins and polysaccharide fibers, scaffolds the matrix and contributes to its mechanical stability, as documented in bacterial biofilm systems [6,7]. Bacteria integrate seamlessly into this microalgal matrix, where they activate their respiration kinetics and secrete enzymatic proteins that stabilize the community structure, as has been shown for mixed seaweed biofilms [63]. Concurrently, fungi act as a physical scaffold, providing crucial mycelial support but becoming progressively less metabolically active as the biofilm matures. Although yeast cells remain numerically abundant during periods of nutrient deprivation, their metabolic activity and overall contribution to extracellular DNA and protein production are low; within complex biofilms, their survival is likely sustained exclusively via beneficial interactions with their symbiotic partners.

Another crucial aspect of these systems under investigation is the extent of physical and metabolic communication between different biofilm components. Scanning electron micrographs confirmed the distinct spatial colocalization of bacteria with microalgae and bacteria with fungi, and to a lesser extent, fungi with yeast. In later stages of biofilm development, the fungal mycelium formed an interconnected network that physically bridged separate microalgal clusters, resembling fungal highways. Furthermore, the hyphae established intimate physical contact with the microalgal cells. Similarly, bacteria formed dense, close associations directly on the surface of the microalgal cell walls. The functional relationship between the bacteria and fungi was further validated by the fact that cumulative biomass within the binary biofilms significantly increased in the presence of the bacterial component.

Summarizing the results of modelling the protolichen biofilm, it can be concluded that, in multi-species biofilms developing under conditions of carbohydrate deficiency—serving as a representative model of a ‘protolichen on a rock’ or a protolichen cenosis—the main functional effectors and moderators of the overall metabolic activity are the *Asterochloris* microalgae (primary producers) and the bacteria. These two components probably trigger complex regulatory-trophic cascades together, modulating the metabolic architecture of the extracellular matrix. In contrast, filamentous fungi primarily play a stabilizing role during the initial stages of colonization, physically anchoring microalgal and bacterial cells to the surface of the forming biofilm substratum.

Interestingly, the yeast component tends to exhibit metabolic inertness during the initial stages of ‘protolichen biofilm’ formation, largely abstaining from matrix biogenesis or early symbiotic partnerships. This behavior could be a sit-and-wait ecological tactic, whereby the yeasts delay active proliferation until the mature consortium generates substantial organic matter. This apparent metabolic passivity suggests either a persistent K-

strategy focused on exploiting metabolites accumulated by the mature community [64,65], or a specialized tactic of delayed parasitism [66,67].

5. Conclusions

In conclusion, the findings of this study suggest that, within the protolichen models investigated, bacteria and microalgae appear to play primary roles in driving biofilm configuration and functional optimization. Conversely, under severe organic carbon deprivation, filamentous fungi experience strictly constrained biomass expansion, while yeast populations are heavily suppressed. The progression of consortium complexity from monocultures to binary and ternary systems appears to trigger distinct emergent effects, potentially enhancing extracellular DNA release and metabolic activity, which seem to function as mutually interdependent parameters. Biofilm structural stabilization during the initial stages of assembly likely relies on fungal-derived polysaccharides, whereas late-stage matrix consolidation seemingly depends on microalgal exopolymers. Within these matrix architectures, the bacterial component may vitalize the biofilm by accelerating overall community metabolic processes. Consequently, under strict carbon limitations, heterotrophic yeast populations appear highly dependent on autotrophic primary producers and fungal scaffolds for essential carbohydrate resources. Ultimately, these multi-component synthetic model systems offer a promising framework for deciphering the specialized contributions of individual microbial groups to the formation, structural maintenance and ecological functioning of complex microbial consortia.

Supplementary Materials: The following supporting information can be downloaded at https://www.mdpi.com/article/10.3390/ecologies7030094/s1. Figure S1: Phylogenetic tree showing the position of algal strain 11A1 among related taxa within the genera *Asterochloris*, *Myrmecia*, and *Trebouxia*, based on chloroplast 23S rRNA gene sequences. The evolutionary history was inferred using the Maximum Likelihood method and the Jukes–Cantor model. The percentage of replicate trees in which the associated taxa clustered together in the bootstrap test (1000 replicates) is shown next to the branches. Representatives of the genus *Trebouxia* were used as an outgroup. The tree is drawn to scale, with branch lengths measured in the number of substitutions per site. Evolutionary analyses were conducted in MEGA X. Figure S2: Phylogenetic tree showing the position of *Gordonia* sp. strain NM9-41 among related taxa within the genus *Gordonia*, based on 16S rRNA gene sequences. The evolutionary history was inferred using the Maximum Likelihood method and the Jukes–Cantor model. The percentage of replicate trees in which the associated taxa clustered together in the bootstrap test (1000 replicates) is shown next to the branches. *Staphylococcus aureus* ATCC 12600 was used as an outgroup. The tree is drawn to scale, with branch lengths measured in the number of substitutions per site. Evolutionary analyses were conducted in MEGA X. Figure S3: Phylogenetic tree showing the position of fungal strain 7.1.2.4 among related taxa within the genus *Thelebolus* and the class *Leotiomycetes*, based on the ITS rRNA region sequences. The evolutionary history was inferred using the Maximum Likelihood method and the Jukes–Cantor model. The percentage of replicate trees in which the associated taxa clustered together in the bootstrap test (1000 replicates) is shown next to the branches. *Catenulifera brachyconia* CBS 700.73 and *Catenulifera brevicollaris* CBS 126.74 were used as an outgroup. The tree is drawn to scale, with branch lengths measured in the number of substitutions per site. Evolutionary analyses were conducted in MEGA X. Figure S4: Phylogenetic tree showing the position of yeast strain 7.1.2.11 among related taxa within the genera *Occultifur* and *Microsporomyces*, based on the ITS rRNA region sequences. The evolutionary history was inferred using the Maximum Likelihood method and the Jukes–Cantor model. The percentage of replicate trees in which the associated taxa clustered together in the bootstrap test (1000 replicates) is shown next to the branches. The tree is drawn to scale, with branch lengths measured in the number of substitutions per site. Evolutionary analyses were conducted in MEGA X. Figure S5: Scanning electron micrographs of monospecies biofilms on the 30th day of incubation, illustrating the extracellular polymeric substance (EPS) matrix formed by *Asterochloris* sp. (a) and *Thelebolus* sp.

(b). Designations: YAS—young aplanospores; MC—mature cells; EPSm—EPS matrix; H1—type I hyphae; H2—type II hyphae. Scale bars: 50 μm. Figure S6: Scanning electron (a) and fluorescence (b) micrographs of *Asterochloris* sp. monospecies biofilms on day 30 of incubation. Designations: YAS—young aplanospores; MC—mature cells. Scale bars: (a)—10 μm; (b)—5 μm. Figure S7: Scanning electron micrographs of binary biofilms (*Thelebolus* sp. and *Asterochloris* sp.) on day 30 of incubation. Designations: CL—mycelial clusters; A—anastomosis; R—ring; H1—type I hyphae; H2—type II hyphae. Magnification and scale bars: (a)—1100×, 10 μm; (b)—500×, 50 μm. Figure S8: Scanning electron micrographs of binary biofilms (*Thelebolus* sp. and *Gordonia* sp.) on days 5 (a,c,e) and 30 (b,d,f) of incubation. Designations: μCol—bacterial microcolonies; YμCol—young bacterial microcolonies; MμCol—mature bacterial microcolonies; FS—cell-free space; BL—bacterial lawn. Scale bars: (a,b)—50 μm; (c,d)—10 μm; (e,f)—5 μm. Figure S9: Scanning electron micrographs of 4-component combined biofilms (*Gordonia* sp., *Occultifur* sp., *Thelebolus* sp., and *Asterochloris* sp.) focusing on yeast cells. Designations: YCM—yeast cells on the matrix; FLYC—free lawn of yeast cells. Magnification and scale bars: 500×, 50 μm. Figure S10: Scanning electron micrographs of mature 4-component biofilms (*Gordonia* sp., *Occultifur* sp., *Thelebolus* sp., and *Asterochloris* sp.) on day 30 of incubation. Designations: BCol—bacterial colonies; MAC—mature algal cell. Magnification and scale bars: (a)—1100×, 10 μm; (b)—3000×, 5 μm.; Figure S11: Heatmap of the specific activity index (SAI) for monospecies, binary, 3-component, and 4-component biofilms depending on exposure time (days). Designations of biofilm types: B—bacteria (*Gordonia* sp.), Y—yeast (*Occultifur* sp.), F—fungi (*Thelebolus* sp.), A—algae (*Asterochloris* sp.). Letter combinations indicate artificial consortia of these organisms.

Author Contributions: Conceptualization, T.A.P.; methodology, T.A.P.; data preparation, A.V.H. and T.A.P.; formal analysis, T.A.P.; investigation, A.V.H. and T.A.P.; data curation, T.A.P.; writing—original draft preparation, T.A.P.; writing—review and editing, A.V.H. and T.A.P.; visualization, A.V.H. and T.A.P.; supervision, T.A.P.; project administration, T.A.P.; funding acquisition, T.A.P. All authors have read and agreed to the published version of the manuscript.

Funding: This research was funded by Russian Science Foundation, grant number 25-24-00195.

Institutional Review Board Statement: Not applicable.

Informed Consent Statement: Not applicable.

Data Availability Statement: The 16S rRNA, 23S rRNA, 18S rRNA (partial), ITS1, 5.8S rRNA, ITS2 and 28S rRNA (partial) gene sequences of pure cultures are deposited in GenBank under the following accession numbers: PZ807577, PZ834537, PZ807174 and PZ838513.

Acknowledgments: The authors would like to express their gratitude to the UNIQEM Shared-Use Centre at the Federal Research Centre for Biotechnology of the Russian Academy of Sciences, and particularly to Vladimir V. Sorokin and Marina Sorokina, for their assistance in the preparation of scanning electron micrographs.

Conflicts of Interest: The authors declare no conflicts of interest.

References

1. Nozhevnikova, A.N.; Botchkova, E.A.; Plakunov, V.K. Multi-Species Biofilms in Ecology, Medicine, and Biotechnology. *Microbiology* **2015**, *84*, 731–750. [CrossRef]
2. Sentenac, H.; Loyau, A.; Leflaive, J.; Schmeller, D.S. The Significance of Biofilms to Human, Animal, Plant and Ecosystem Health. *Funct. Ecol.* **2022**, *36*, 294–313. [CrossRef]
3. Oster, S.; Bollinger, E.; Schreiner, V.C.; Schmitt, T.; Filker, S.; Bundschuh, M. Functional Stability despite Structural Changes in Freshwater Biofilm Communities Exposed to an Antibiotic and an Herbicide—The Role of Nutrient Conditions. *FEMS Microbiol. Ecol.* **2025**, *101*, fiaf094. [CrossRef]
4. Davey, M.E.; O'toole, G.A. Microbial Biofilms: From Ecology to Molecular Genetics. *Microbiol. Mol. Biol. Rev.* **2000**, *64*, 847–867. [CrossRef] [PubMed]

5. Gannesen, A.V.; Ziganshin, R.H.; Ovcharova, M.A.; Mosolova, A.M.; Loginova, N.A.; Diuvenji, E.V.; Nevolina, E.D.; Mart'yanov, S.V.; Plakunov, V.K. Changes in the Protein Profiles of Staphylococcus Epidermidis Planktonic Cultures and Biofilms under Anoxic Conditions in the Presence of the CNP Hormone. *Microbiology* **2024**, *93*, 799–811. [CrossRef]
6. Flemming, H.-C.; van Hullebusch, E.D.; Neu, T.R.; Nielsen, P.H.; Seviour, T.; Stoodley, P.; Wingender, J.; Wuertz, S. The Biofilm Matrix: Multitasking in a Shared Space. *Nat. Rev. Microbiol.* **2023**, *21*, 70–86. [CrossRef] [PubMed]
7. Böhning, J.; Tarafder, A.K.; Bharat, T.A.M. The Role of Filamentous Matrix Molecules in Shaping the Architecture and Emergent Properties of Bacterial Biofilms. *Biochem. J.* **2024**, *481*, 245–263. [CrossRef] [PubMed]
8. Spribille, T.; Tagirdzhanova, G.; Goyette, S.; Tuovinen, V.; Case, R.; Zandberg, W.F. 3D Biofilms: In Search of the Polysaccharides Holding Together Lichen Symbioses. *FEMS Microbiol. Lett.* **2020**, *367*, fnaa023. [CrossRef] [PubMed]
9. Carr, E.C.; Harris, S.D.; Herr, J.R.; Riekhof, W.R. Lichens and Biofilms: Common Collective Growth Imparts Similar Developmental Strategies. *Algal Res.* **2021**, *54*, 102217. [CrossRef]
10. Aschenbrenner, I.A.; Cernava, T.; Berg, G.; Grube, M. Understanding Microbial Multi-Species Symbioses. *Front. Microbiol.* **2016**, *7*, 180. [CrossRef] [PubMed]
11. Hawksworth, D.L.; Grube, M. Lichens Redefined as Complex Ecosystems. *New Phytol.* **2020**, *227*, 1281–1283. [CrossRef] [PubMed]
12. Pichler, G.; Muggia, L.; Carniel, F.C.; Grube, M.; Kranner, I. How to Build a Lichen: From Metabolite Release to Symbiotic Interplay. *New Phytol.* **2023**, *238*, 1362–1378. [CrossRef] [PubMed]
13. Ahmadjian, V. Artificial Reestablishment of the Lichen Cladonia Cristatella. *Science* **1966**, *151*, 199–201. [CrossRef] [PubMed]
14. Ahmadjian, V. Lichen Synthesis. *Österr. Bot. Z.* **1969**, *116*, 306–311. [CrossRef]
15. Honegger, R. Lichens and Their Allies Past and Present. In *Plant Relationships: Fungal-Plant Interactions*; Scott, B., Mesarich, C., Eds.; Springer International Publishing: Cham, Switzerland, 2023; pp. 133–183.
16. Kono, M.; Kon, Y.; Ohmura, Y.; Satta, Y.; Terai, Y. In Vitro Resynthesis of Lichenization Reveals the Genetic Background of Symbiosis-Specific Fungal-Algal Interaction in Usnea Hakonensis. *BMC Genom.* **2020**, *21*, 671. [CrossRef] [PubMed]
17. Pichler, G.; Candotto Carniel, F.; Muggia, L.; Holzinger, A.; Tretiach, M.; Kranner, I. Enhanced Culturing Techniques for the Mycobiont Isolated from the Lichen Xanthoria Parietina. *Mycol. Prog.* **2021**, *20*, 797–808. [CrossRef] [PubMed]
18. Puginier, C.; Libourel, C.; Otte, J.; Skaloud, P.; Haon, M.; Grisel, S.; Petersen, M.; Berrin, J.-G.; Delaux, P.-M.; Dal Grande, F.; et al. Phylogenomics Reveals the Evolutionary Origins of Lichenization in Chlorophyte Algae. *Nat. Commun.* **2024**, *15*, 4452. [CrossRef]
19. Kim, W.; Jeong, M.-H.; Yun, S.-H.; Hur, J.-S. Transcriptome Analysis Identifies a Gene Cluster for the Biosynthesis of Biruloquinone, a Rare Phenanthraquinone, in a Lichen-Forming Fungus Cladonia Macilenta. *J. Fungi* **2021**, *7*, 398. [CrossRef]
20. Grube, M.; Berg, G. Microbial Consortia of Bacteria and Fungi with Focus on the Lichen Symbiosis. *Fungal Biol. Rev.* **2009**, *23*, 72–85. [CrossRef]
21. Bates, S.T.; Cropsey, G.W.G.; Caporaso, J.G.; Knight, R.; Fierer, N. Bacterial Communities Associated with the Lichen Symbiosis. *Appl. Environ. Microbiol.* **2011**, *77*, 1309–1314. [CrossRef]
22. Grimm, M.; Grube, M.; Schiefelbein, U.; Zühlke, D.; Bernhardt, J.; Riedel, K. The Lichens' Microbiota, Still a Mystery? *Front. Microbiol.* **2021**, *12*, 623839. [CrossRef] [PubMed]
23. Díaz, E.-M.; Rodríguez, S.; Quintana, J. Epiphytic Bacteria on Lichens. In *Biochemical Responses of Plants to Invaders*; Research Signpost: Kerala, India, 2008; pp. 1–12.
24. Honegger, R. The Symbiotic Phenotype of Lichen-Forming Ascomycetes and Their Endo- and Epibionts. In *Fungal Associations*; Hock, B., Ed.; Springer: Berlin/Heidelberg, Germany, 2012; pp. 287–339.
25. Kachalkin, A.; Tomashevskaya, M.; Pankratov, T.; Yurkov, A. Endothallic Yeasts in the Terricolous Lichens *Cladonia*. *Mycol. Prog.* **2024**, *23*, 29. [CrossRef]
26. Schwob, G.; Almendras, K.; Veas-Mattheos, K.; Pezoa, M.; Orlando, J. Host Specialization and Spatial Divergence of Bacteria Associated with Peltigera Lichens Promote Landscape Gamma Diversity. *Environ. Microbiome* **2024**, *19*, 57. [CrossRef] [PubMed]
27. Lagarde, A.; Jargeat, P.; Roy, M.; Girardot, M.; Imbert, C.; Millot, M.; Mambu, L. Fungal Communities Associated with *Evernia prunastri*, *Ramalina fastigiata* and *Pleurosticta acetabulum*: Three Epiphytic Lichens Potentially Active against *Candida* Biofilms. *Microbiol. Res.* **2018**, *211*, 1–12. [CrossRef] [PubMed]
28. Pushpavathi, D.; Krishnamurthy, Y.L. Study on Endolichenic Fungal Assemblage in Parmotrema and Heterodermia Lichens of Shivamoga, Karnataka. *Mol. Biol. Rep.* **2024**, *51*, 549. [CrossRef]
29. Moya, P.; Molins, A.; Martínez-Alberola, F.; Muggia, L.; Barreno, E. Unexpected Associated Microalgal Diversity in the Lichen Ramalina Farinacea Is Uncovered by Pyrosequencing Analyses. *PLoS ONE* **2017**, *12*, e0175091. [CrossRef] [PubMed]
30. Silverstein, M.R.; Bhatnagar, J.M.; Segrè, D. Metabolic Complexity Drives Divergence in Microbial Communities. *Nat. Ecol. Evol.* **2024**, *8*, 1493–1504. [CrossRef] [PubMed]
31. Wang, M.; Chen, X.; Fang, Y.; Zheng, X.; Huang, T.; Nie, Y.; Wu, X.-L. The Trade-off between Individual Metabolic Specialization and Versatility Determines the Metabolic Efficiency of Microbial Communities. *Cell Syst.* **2024**, *15*, 63–74.e5. [CrossRef] [PubMed]
32. Flemming, H.-C.; Wingender, J.; Szewzyk, U.; Steinberg, P.; Rice, S.A.; Kjelleberg, S. Biofilms: An Emergent Form of Bacterial Life. *Nat. Rev. Microbiol.* **2016**, *14*, 563–575. [CrossRef] [PubMed]

33. Flaig, M.L.; Amador, C.I.; Burmølle, M. Multispecies Biofilms Are Hubs for Metabolic Interactions Leading to Ecologically and Biotechnologically Relevant Emergent Properties. *Curr. Opin. Microbiol.* **2026**, *92*, 102776. [CrossRef] [PubMed]
34. Ametrano, C.G.; Selbmann, L.; Muggia, L. A Standardized Approach for Co-Culturing Dothidealean Rock-Inhabiting Fungi and Lichen Photobionts in Vitro. *Symbiosis* **2017**, *73*, 35–44. [CrossRef]
35. Azeredo, J.; Azevedo, N.F.; Briandet, R.; Cerca, N.; Coenye, T.; Costa, A.R.; Desvaux, M.; Di Bonaventura, G.; Hébraud, M.; Jaglic, Z.; et al. Critical Review on Biofilm Methods. *Crit. Rev. Microbiol.* **2017**, *43*, 313–351. [CrossRef] [PubMed]
36. Wilson, C.; Lukowicz, R.; Merchant, S.; Valquier-Flynn, H.; Caballero, J.; Sandoval, J.; Okuom, M.; Huber, C.; Brooks, T.D.; Wilson, E.; et al. Quantitative and Qualitative Assessment Methods for Biofilm Growth: A Mini-Review. *Res. Rev. J. Eng. Technol.* **2017**, *6*, 1–25. Available online: https://pmc.ncbi.nlm.nih.gov/articles/PMC6133255/ (accessed on 27 August 2026). [PubMed] [PubMed Central]
37. Relucenti, M.; Familiari, G.; Donfrancesco, O.; Taurino, M.; Li, X.; Chen, R.; Artini, M.; Papa, R.; Selan, L. Microscopy Methods for Biofilm Imaging: Focus on SEM and VP-SEM Pros and Cons. *Biology* **2021**, *10*, 51. [CrossRef]
38. Agarwal, H.; Gurnani, B.; Pippal, B.; Jain, N. Capturing the Micro-Communities: Insights into Biogenesis and Architecture of Bacterial Biofilms. *BBA Adv.* **2025**, *7*, 100133. [CrossRef] [PubMed]
39. Neu, T.R.; Kuhlicke, U. Biofilm Analysis by Confocal Microscopy—Basics and Practical Aspects. *Microsc. Res. Tech.* **2026**, *89*, 183–206. [CrossRef] [PubMed]
40. Hakobjanyan, A.; Melekhin, A.; Sukhacheva, M.; Beletsky, A.; Pankratov, T. Mycobiomes of Six Lichen Species from the Russian Subarctic: A Culture-Independent Analysis and Cultivation Study. *J. Fungi* **2025**, *11*, 848. [CrossRef] [PubMed]
41. Schoutteten, N.; Yurkov, A.; Spirin, V.; Savchenko, A.; Aime, M.C.; Begerow, D.; Verbeken, A. Examination of Mycoparasites Reveals a New Type of Host-Parasite Interface and Rearranges the Taxonomy of *Occultifur* and *Microsporomyces* (*Cystobasidiomycetes*, *Basidiomycota*). *Stud. Mycol.* **2024**, *109*, 451–486. [CrossRef] [PubMed]
42. Stein, J.R. (Ed.) *Handbook of Phycological Methods: Culture Methods and Growth Measurements*; Cambridge University Press: Cambridge, UK, 1973.
43. White, T.J.; Bruns, T.; Lee, S.; Taylor, J. 38—Amplification and Direct Sequencing of Fungal Ribosomal RNA Genes for Phylogenetics. In *PCR Protocols*; Innis, M.A., Gelfand, D.H., Sninsky, J.J., White, T.J., Eds.; Academic Press: San Diego, CA, USA, 1990; pp. 315–322.
44. Vilgalys, R.; Hester, M. Rapid Genetic Identification and Mapping of Enzymatically Amplified Ribosomal DNA from Several Cryptococcus Species. *J. Bacteriol.* **1990**, *172*, 4238–4246. [CrossRef] [PubMed]
45. Rehner, S.A.; Samuels, G.J. Taxonomy and Phylogeny of *Gliocladium* Analysed from Nuclear Large Subunit Ribosomal DNA Sequences. *Mycol. Res.* **1994**, *98*, 625–634. [CrossRef]
46. Lane, D.J. 16S/23S rRNA Sequencing. In *Nucleic Acid Techniques in Bacterial Systematics*; Stackebrandt, E., Goodfellow, M., Eds.; John Wiley and Sons: New York, NY, USA, 1991; pp. 115–175.
47. del Campo, E.M.; Casano, L.M.; Gasulla, F.; Barreno, E. Suitability of Chloroplast LSU rDNA and Its Diverse Group I Introns for Species Recognition and Phylogenetic Analyses of Lichen-Forming *Trebouxia* Algae. *Mol. Phylogenet. Evol.* **2010**, *54*, 437–444. [CrossRef] [PubMed]
48. Kumar, S.; Stecher, G.; Li, M.; Knyaz, C.; Tamura, K. MEGA X: Molecular Evolutionary Genetics Analysis across Computing Platforms. *Mol. Biol. Evol.* **2018**, *35*, 1547–1549. [CrossRef] [PubMed]
49. Bakken, L.R.; Olsen, R.A. Buoyant Densities and Dry-Matter Contents of Microorganisms: Conversion of a Measured Biovolume into Biomass. *Appl. Environ. Microbiol.* **1983**, *45*, 1188–1195. [CrossRef] [PubMed]
50. Wells, M.; Mikesh, M.; Gordon, V. Structure-Preserving Fixation Allows Scanning Electron Microscopy to Reveal Biofilm Microstructure and Interactions with Immune Cells. *J. Microsc.* **2024**, *293*, 59–68. [CrossRef] [PubMed]
51. Corte, L.; Casagrande Pierantoni, D.; Tascini, C.; Roscini, L.; Cardinali, G. Biofilm Specific Activity: A Measure to Quantify Microbial Biofilm. *Microorganisms* **2019**, *7*, 73. [CrossRef] [PubMed]
52. Mukhopadhyay, S.K.; Chatterjee, S.; Gauri, S.S.; Das, S.S.; Mishra, A.; Patra, M.; Ghosh, A.K.; Das, A.K.; Singh, S.M.; Dey, S. Isolation and Characterization of Extracellular Polysaccharide Thelebolan Produced by a Newly Isolated Psychrophilic Antarctic Fungus Thelebolus. *Carbohydr. Polym.* **2014**, *104*, 204–212. [CrossRef] [PubMed]
53. Leibly, D.J.; Nguyen, T.N.; Kao, L.T.; Hewitt, S.N.; Barrett, L.K.; Voorhis, W.C.V. Stabilizing Additives Added during Cell Lysis Aid in the Solubilization of Recombinant Proteins. *PLoS ONE* **2012**, *7*, e52482. [CrossRef] [PubMed]
54. Tokmakov, A.A.; Kurotani, A.; Sato, K.-I. Protein pI and Intracellular Localization. *Front. Mol. Biosci.* **2021**, *8*, 775736. [CrossRef] [PubMed]
55. Palková, Z.; Váchová, L. Cell Differentiation, Aging, and Death in Spatially Organized Yeast Communities: Mechanisms and Consequences. *Cell Death Differ.* **2025**, *32*, 1557–1569. [CrossRef] [PubMed]
56. Rather, M.A.; Gupta, K.; Mandal, M. Microbial Biofilm: Formation, Architecture, Antibiotic Resistance, and Control Strategies. *Braz. J. Microbiol.* **2021**, *52*, 1701–1718. [CrossRef] [PubMed]

57. Flynn, K.J.; Clark, D.R.; Xue, Y. Modeling the Release of Dissolved Organic Matter by Phytoplankton. *J. Phycol.* **2008**, *44*, 1171–1187. [CrossRef] [PubMed]
58. Villacorte, L.O.; Ekowati, Y.; Neu, T.R.; Kleijn, J.M.; Winters, H.; Amy, G.; Schippers, J.C.; Kennedy, M.D. Characterisation of Algal Organic Matter Produced by Bloom-Forming Marine and Freshwater Algae. *Water Res.* **2015**, *73*, 216–230. [CrossRef] [PubMed]
59. Suzina, N.E.; Sorokin, V.V.; Polivtseva, V.N.; Klyueva, V.V.; Emelyanova, E.V.; Solyanikova, I.P. From Rest to Growth: Life Collisions of Gordonia Polyisoprenivorans 135. *Microorganisms* **2022**, *10*, 465. [CrossRef] [PubMed]
60. Tolker-Nielsen, T.; Molin, S. Spatial Organization of Microbial Biofilm Communities. *Microb. Ecol.* **2000**, *40*, 75–84. [CrossRef] [PubMed]
61. Liu, W.; Røder, H.L.; Madsen, J.S.; Bjarnsholt, T.; Sørensen, S.J.; Burmølle, M. Interspecific Bacterial Interactions Are Reflected in Multispecies Biofilm Spatial Organization. *Front. Microbiol.* **2016**, *7*, 213013. [CrossRef] [PubMed]
62. de Plano, L.M.; Caratozzolo, M.; Conoci, S.; Guglielmino, S.P.P.; Franco, D. Impact of Nutrient Starvation on Biofilm Formation in Pseudomonas Aeruginosa: An Analysis of Growth, Adhesion, and Spatial Distribution. *Antibiotics* **2024**, *13*, 987. [CrossRef] [PubMed]
63. Lipsman, V.; Shlakhter, O.; Rocha, J.; Segev, E. Bacteria Contribute Exopolysaccharides to an Algal-Bacterial Joint Extracellular Matrix. *npj Biofilms Microbiomes* **2024**, *10*, 36. [CrossRef] [PubMed]
64. Qiao, Y.; Sun, Y.; Shen, M.; Kong, L.; Gao, Y.; Cheng, D.; Zhu, W.; Li, C.; Liu, Y. Bacterial K-Strategists Playing Pivotal Roles in Degrading Alkanes, Upholding System Stability and Regulating Microbial Diversity in Natural Attenuation of Petroleum Hydrocarbon Polluted Sediment of Laizhou Bay. *J. Environ. Manag.* **2025**, *393*, 126958. [CrossRef] [PubMed]
65. Luo, L.; Chen, X.; Liu, B.; Nie, Y.; Wu, X.-L. Strengthen or Weaken: Evolutionary Directions of Cross-Feeding After Formation. *Environ. Microbiol. Rep.* **2025**, *17*, e70175. [CrossRef] [PubMed]
66. Drew, G.C.; Stevens, E.J.; King, K.C. Microbial Evolution and Transitions along the Parasite–Mutualist Continuum. *Nat. Rev. Microbiol.* **2021**, *19*, 623–638. [CrossRef] [PubMed]
67. Lee, Y.-H.; Lin, W.-J.; Tsai, M.-T.; Lan, B.; Chu, Y.-L.; Yang, J.-I.; Sun, S.-J. Context-Dependent Indirect Effects Mediate Ecological Transitions between Parasitism and Mutualism. *Commun. Biol.* **2026**, *9*, 706. [CrossRef] [PubMed]

Disclaimer/Publisher's Note: The statements, opinions and data contained in all publications are solely those of the individual author(s) and contributor(s) and not of MDPI and/or the editor(s). MDPI and/or the editor(s) disclaim responsibility for any injury to people or property resulting from any ideas, methods, instructions or products referred to in the content.